NUMERICAL MODELING OF WELLBORE INSTABILITY (TENSILE FAILURE) USING FRACTURE MECHANICS APPROACH

BY

JOSSOU ERICMOORE ELIJAH

A THESIS

SUBMITTED TO THE GRADUATE FACULTY

IN PARTIAL FULFILLMENT OF THE REQUIREMENT FOR THE

DEGREE OF

MASTER OF SCIENCE

(Material Science and Engineering)

SUPERVISOR: PROF. WINSTON O. SOBOYEJO

MAY 2013

DECLARATION

I hereby declare that the matter embodied in this thesis entitled "Numerical Modeling of Wellbore Instability (Tensile Failure) Using Fracture Mechanics Approach" is the result of investigation carried out by me under the supervision of Professor Winston O. Soboyejo at African University of Science and Technology, Abuja and that it has not been submitted elsewhere for the award of any degree or diploma.

In keeping with the general practice in reporting scientific observation, due acknowledgement has been made whenever the work described is based on the findings of other investigators.

_____

Jossou Ericmoore Elijah

CERTIFICATION

We hereby certify that the matter embodied in this thesis entitled "Numerical Modeling of Wellbore Instability (Tensile Failure) Using Fracture Mechanics Approach" has been carried out by Mr. Jossou Ericmoore Elijah, at African University of Science and Technology, Abuja under the supervision of Professor Winston O. Soboyejo and that it has not been submitted elsewhere for the award of any degree or diploma.

Supervisor: _____
Prof. Wole Soboyejo

ACKNOWLEDGEMENTS

It is impossible to adequately appreciate the people who supported me through what has been the most academically challenging years of my life. Any success that I achieve today can be attributed to the selfless disposition and attitude of the various people God has placed in my life.

Special thanks to my supervisor, Professor Winston O. Soboyejo, for providing me with the opportunity and means to grow and thrive under his guidance. He has inspired me with his success story and disposition to science and life generally. He has taught me that limits are self-imposed, and should always be challenged. He has provided me with strong leadership and direction in the bid to achieve a milestone in my research quest and scientific development. Beyond his role as a supervisor, he has been a father in every sense of it to me.

In addition, I extend my appreciation to Dr. Apheus Igbokoyi and Dr. Omololu Akin-Ojo, for contributing to the success of this work. Dr. Igbokoyi out of his busy schedule makes out time to come to AUST to enlighten us about the grey areas in this work. There is never a moment I go to Dr. Omololu's office that he will not ask about my work and offer advice that have find useful in the completion of this work.

I would also like to acknowledge the support I received from my classmates and members of the multifunctional research group. Mr. Ebenezer Annan has been a great support in the group. He single handedly kept the weekly presentation of the group running and meaningful. Ifeanyi Kalu my research partner has been a tremendous help and inspiration. His meticulous and careful ways of analyzing problems, brought a dynamic to our work and reflect in the quality of work we have done.

Mr. Oyewole Kehinde and Mr. Malik Idris have been of tremendous help in the use of ABAQUS. I am in awe of their intellect, and the way they choose to share it. They made the work easier for me with the insight into fundamentals of fracture mechanics and its applications to various materials.

Great thanks to my parents, Mr. and Mrs. Jossou. They have been a source of encouragement these past years. Their support for my academic pursuit equals none and their interest in my career development has been a source of motivation likewise. My siblings have also been an integral part of the reason why I strive for mastery and excellence. Thank you for believing in me.

Last, I thank the one who will come first for the rest of my life. Oyenike Jimada, my fiancé and future wife, who has unselfishly given more of herself than I ever had the right to ask. Without her support, I would have fallen long ago. I am grateful to her parents and her siblings, for making me feel like part of their family.

TABLE OF CONTENTS

PAGE

LIST OF TABLES

TABLE **PAGE**

LIST OF FIGURES

FIGURE **PAGE**

ABSTRACT

When a well is drilled, the equilibrium in-situ stress is changed. In order to support the stress relief induced by the drilling and to prevent hydrocarbon influx into the cavity, the borehole is filled with a fluid. These operations create new stress configurations. The main point in wellbore projects is the definition of the drilling fluid density to keep the wellbore stable. The lower bound to the fluid density is the collapse stress that is the limit to shearing. The upper bound is the fracture stress that limits the tensile failure. The fluid densities between these limits is named safe mud weight window. Conventional wellbore stability analysis usually considers the effects of shear or tensile failure using failure criteria that are modeled based on the strength of the formation. This thesis uses numerical finite element method techniques to simulate cracking phenomena that can lead to instability of well configurations within and between shale formations that are relevant to oil wells under pressure. The range of critical conditions associated with possible crack lengths are established by equating the computed crack driving forces to the ranges of published fracture toughness data reported in earlier studies. The ranges of pressures associated with upper mud weight drilling pressure are thus established and compared with the prediction from empirical theories.

CHAPTER ONE

1.1 Background and Introduction

Wellbore stability is a serious drilling problem that cost the oil and gas industry over $500 - $1000 million each year. It is also reported that shale account for 75% of all formations drilled by the oil and gas sector, and 90% of wellbore stability problem occur mainly in the shale formations (Lal et al,1999).

Wellbore instability has become an increasing concern for horizontal and extended reach wells, especially with the move towards completely open hole lateral section, and in some cases, open hole build-up section through shale cap rocks (Tan et al, 2004). More recent drilling innovations such as underbalanced drilling techniques, high pressure jet drilling, re-entry horizontal wells and multiple laterals from a single vertical or horizontal well often give rise to challenging wellbore stability question (Kristiansen, 2004).

Over there years model have been developed to solve the problems associated with shale instability though limited, the models do not capture the varying mechanical properties over the depths of the wells. At present, the mechanical property measurements are made on core samples that are expensive to extract and test using convectional mechanical testing approach. Interlaminar fracture in the shale formations is also difficult to model using available strength-based models.

Fracture mechanics approach can be used in determining mechanical properties of rocks such as Compressive Strength, Young's moduli and fracture toughness using cuttings that are

obtain during convectional drilling operations. These approaches give room for measurement of rock mechanical properties across layers that are relevant for predicting wellbore stability and Interlaminar failure. Results obtained from using this approach can be incorporated into modeling software such as ABAQUS CAE 6.12 (teaching Edition) for predicting wellbore instability under different drilling conditions.

This work will focus on mechanical wellbore stability under conditions that result in failure in the rock formation due to fracture. Conditions such as mixed mode (axial versus shear) loading, mud window weight will be studied to understand their effect on wellbore instability.

1.2 PROBLEM STATEMENT

Over the years, various models have been developed for tackling the problem of wellbore stability, but these models have a number of shortcomings that necessitate this research work. Many of the models presently used make the following assumptions that are not necessarily true in reality;

- Rock is a continuous materials,
- Borehole failure is normally based on single initial failure point.
- Rock is an homogeneous material

Many of the models are fanciful and require so many parameters and computation that make them less attractive to drillers who are trying to reduce the downtime to the barest minimum. The

models depend on data from the core which are usually not real time in tackling the wellbore problem.

1.3 SCOPE of WORK

This study will focus on mechanical wellbore instability and the following areas will be explore

1. The effects of mixed mode (axial versus shear) loading conditions that is relevant to horizontal and vertical wells.
2. The effects of notches and cracks will also be explored to provide insights into the different types of rock defects that can give rise to wellbore instability.
3. The SEM image of fractured shales will be studied to get insight the crack propagation of the shale materials.
4. Rock mechanical properties of the shale will be obtained from cuttings rather than core to make the analysis near real time for making appropriate drilling and production decision on the field.
5. The results of rock mechanical properties measured will be incorporated into fracture mechanics models for prediction of unstable crack growth from notches and cracks that can be formed due to hydraulic fracture.
6. The results of rock mechanical properties measured (Young's Moduli, Compressive strength and fracture toughness) will also be incorporated into finite element models of wellbore structure with horizontal and vertical configuration. The models will be developed within a commercial Finite Element Analysis software package, ABAQUS or ANSYS to determine the window mud pressure for safe drilling.

Over the years, the Rock Mechanics Society has developed various models for predicting wellbore instability towards the successful drilling of hydrocarbon wells in oil and gas industry. The first model based on rock mechanics was developed by Bradley in 1979. Bradley developed borehole failure criteria for the borehole instability problem of inclined wellbores by a semi-empirical approach. The effect of fluid flow into the formation was not involved in the evaluation of stress field on the borehole wall (Hsiao, 1988).

REFERENCE

Kristiansen, T.G. (2004): Drilling Wellbore Stability in the Compacting and Subsiding Valhall Field, paper IADC/SPE 87221 presented at the IADC/SPE Drilling Conference, 2-4 March, Dallas, Texas, U.S.A.

Lal, M., (1999): Drilling Fluid Interaction and Shale Strength, Paper SPE 62800-MS presented at 1999 SPE Latin American and Caribbean Petroleum Engineering Conference, 21-23 April, Carcas, VeneZuela.

Tan, C.P., Yaakub, M.A., Chen, X., Willoughby, D.R., Choi, S.K., Wu, B. (2004): Wellbore Sability of Extended Reach Wells in an Oil Field in Sarawak Basin, South China Sea, paper SPE 88609 presented at the SPE Asia Pacific Oil and Gas Conference and Exhibition, 18-20 October, Perth, Australia.

CHAPTER 2

2.0 Theoretical Background and Literature Review

2.1 Wellbore Stability

Wellbore stability is the term used in the oil and gas industry to describe usable condition of the borehole during drilling operations. A usable hole must accommodate logging or any open hole evaluation, casing run and any other drilling activities trouble free. Wellbore instability occurs when there is either breakout or borehole collapse. Wellbore is classified as either mechanical or chemical depending on the source of the problem.

2.1.1 Chemical Wellbore Instability

Chemical wellbore instability, often called shale instability which arise from damaging interaction between the rock, generally shale, and the drilling fluid (Martins et al, 1999). Flow of water into or out of shales is somewhat similar in mechanism to the flow of water through a semi-permeable membrane (osmosis). Osmosis is the flow of solvent (water) from a solution containing lower concentration of solute (salinity) into a solution of higher solute concentration through a membrane that is permeable to the solvent but not to the solute. The pressure required to prevent water from moving through a semi-permeable membrane from a solution of low salinity to a solution of high salinity is called osmotic pressure.

The driving forces involved in solute and solvent transport through a membrane are the chemical potential gradients across the membrane. Since these are not measurable quantities, driving forces for osmosis are generally related to differences in solute concentration (water activities) and pressure across the membrane (Mody et al, 1996).

The final equilibrium osmotic pressure, however, not only depends on the difference in the activity of the drilling fluid and the shale but also depends on the reflection coefficient. For an ideal semi-permeable membrane, the reflection coefficient is equal to unity indicating all solute is reflected by the membrane and only water molecules can pass through the membrane. When the reflection coefficient is equal to zero, there is no osmotic flow and the solute and solvent can flow freely across the membrane.

Shale is not an ideal semi-permeable membrane to water based solutions because it has a range of pore size distribution including wide pore throats which result in significant permeability to solute. As the pore size decreases the solute interacts more strongly with the pore walls which reduce the permeability of the membrane to the solute. This will result in an increase in the reflection coefficient of the shale.

When the activity of the drilling fluid is lower than the shale activity, an osmotic backflow of pore fluid from the formation will reduce the rate of pore pressure increase due to hydraulic gradient. If the osmotic backflow is greater than the flow due to hydraulic gradient, there will be a net flow of water out of the formation into the wellbore. This will result in the dehydration of the formation and lowering of the pore pressure below the in-situ value. The associated increase in the formation strength and effective mud support pressure lead to an improvement in the stability of the wellbore. However, excessive dehydration of shales can cause a decrease in the formation strength which reduces (or may even negate) the wellbore stability improvement (Mody et al, 1993). For reflection coefficients of less than unity (’leaky’ membrane), some solutes are transferred across the membrane system which would eventually eliminate the chemical potential/activity imbalance between the drilling fluid and

the shale. Hence, osmotic backflow of pore fluid from the formation across a 'leaky' membrane would only provide a temporary mechanism (Chee et al, 1996).

2.1.2 Mechanical Wellbore Instability

Mechanical wellbore instability is basically a contest between the strength of the in-situ rock and the stresses induced on it while it is being drilled. Key parameters causing mechanical instability are orientation and magnitude of in-situ stresses, rock strength and properties and drilling practices (Osisanya, 2012).

Mechanical wellbore instability can be broadly classified as being either tensile or compressive. Tensile failure occurs when the pore pressure increases so as to exceed the tensile strength of the rock while compressive failure occurs when there is insufficient wellbore pressure support. This can lead to sloughing in brittle formation, resulting in wellbore enlargement. If the formation behaves plastically, it will flow in the hole resulting into hole tightening. Borehole instability problem can therefore be classified into the following categories based on the magnitude of the mud weight magnitudes (Lang et al, 2011).

1. Wellbore washout or kicks owing to underbalanced drilling, where the mud weight is far less than pore pressure, or a result of drilling in unconsolidated or weak formations.

2. Breakouts or shear failures owing to low mud weight.

3. Losses or lost circulation from high mud weight.

4. Failures or sliding related to pre-existing fractures or drilling-induced formation damage.

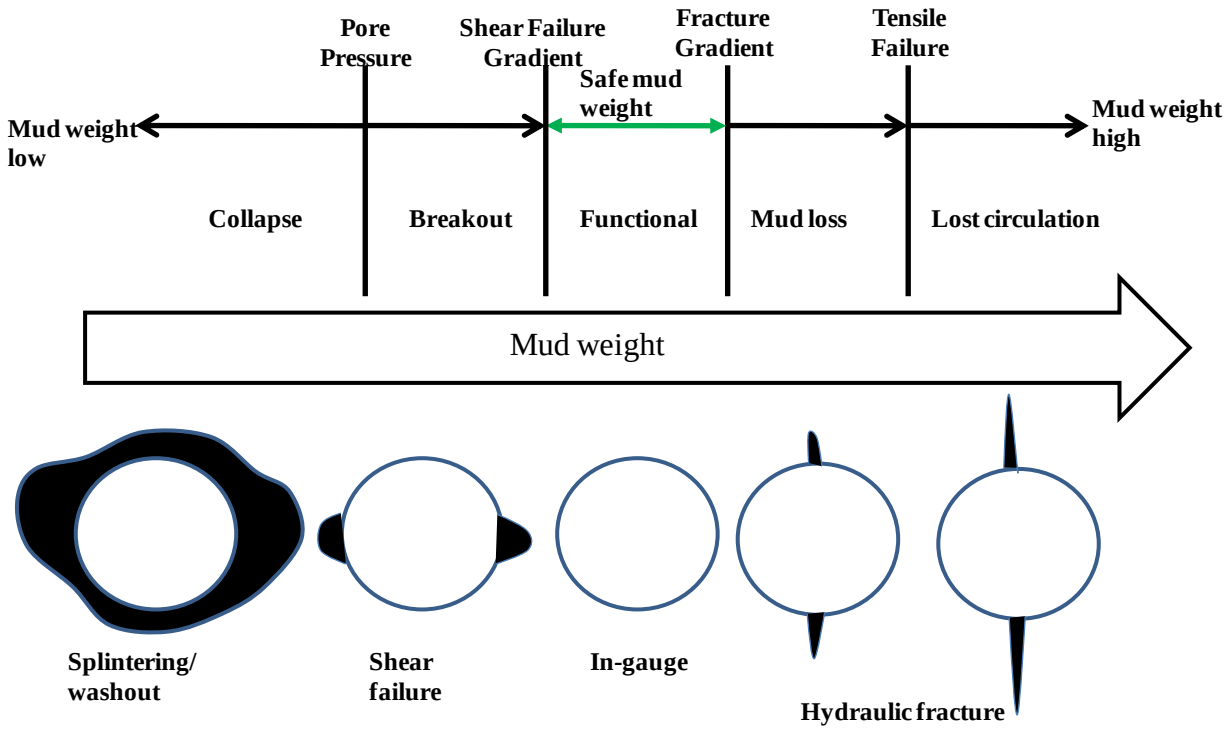

Figure 2.1: Schematic relationship of mud pressure (mud weight) and wellbore failure (Lang et al, 2011).

2.2 Understanding Subsurface Shale

Shale is a fine-grained sedimentary rock often composed of clay and other minerals. The predominance of clays influences its mechanical properties and typically imparts a strong elastic anisotropy. Shales are often rich in organic material called kerogen which acts as a source during hydrocarbon generation. Shale formations are interesting to the oil and gas industry because they host vast natural gas and oil resources. Gas flows to the wellbore primarily through natural and

induced fractures. The natural fractures are caused by tectonic forces, desiccation and hydrocarbon generation while the process of hydraulic fracturing stimulates and induces fractures.

The distinguishing features of shale (of interest to oil industry) are its clay content, low permeability (independent of porosity) due to poor pore connectivity through narrow pore throats (typical pore diameters range 3 nm-100 nm with largest number of pores having 10 nm diameter), and large difference in the coefficient of thermal expansion between water and the shale matrix constituents.

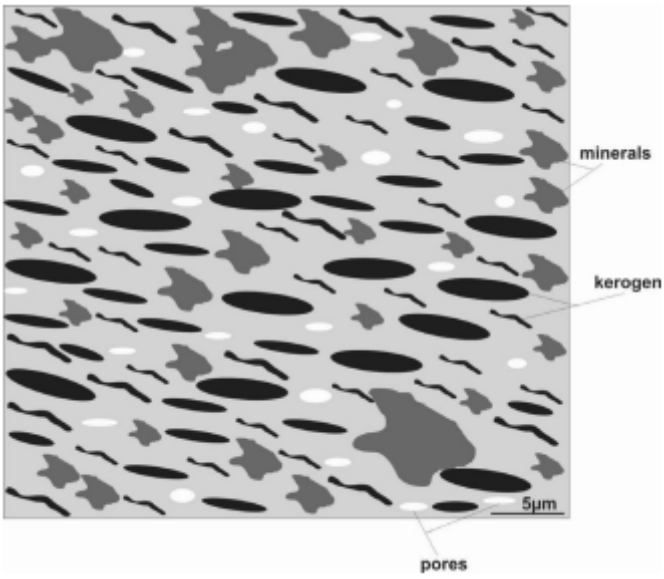

Figure 2.2: Sketches Illustrating the Principal Volumetric Components of Shale (Potter et al, 1984)

2.3 Wellbore stresses – model development In Oil Well

The rock formation is in a state of equilibrium until a wellbore is drilled. The stresses in the earth under these conditions are known as the far field stresses (σ_v, σ_H, σ_h) or *in-situ* stresses (Gaurina,

1994). When the well is drilled, the rock stresses in the vicinity of the wellbore are redistributed as the support originally offered by the drilled out rock is replaced by the hydraulic pressure of the mud. The stresses can be resolved into a vertical or overburden stress, σ_v, and two horizontal stresses, σ_H (the maximum horizontal *in-situ* stress), and σ_h (the minimum horizontal *in-situ* stress), which are generally unequal (**Figure 2.3**) (McLean et al, 1990).

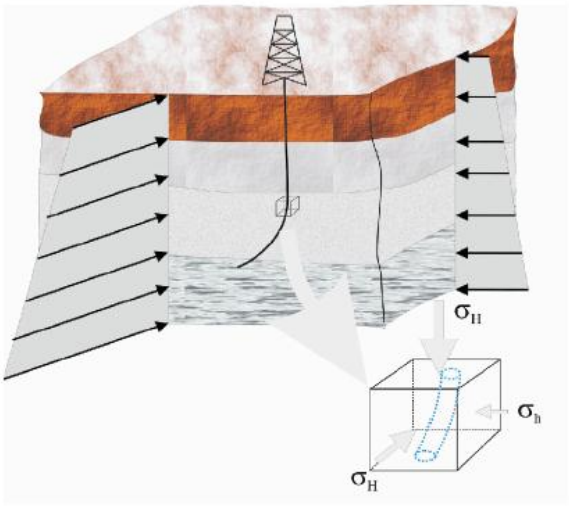

Figure 2.3: *In-situ* stresses

If the redistributed stress state exceeds the rock strength, either in tension or compression, then instability may result. **Figure 2.4** shows the wellbore stresses after drilling. These are described as radial stress σ_r, tangential stress (circumferential or hoop stress) σ_t, and axial stress σ_a. The radial stress acts in all directions perpendicular to the wellbore wall, the tangential stress circles the borehole and the axial stress act parallel to the wellbore axis (McLean et al, 1990).

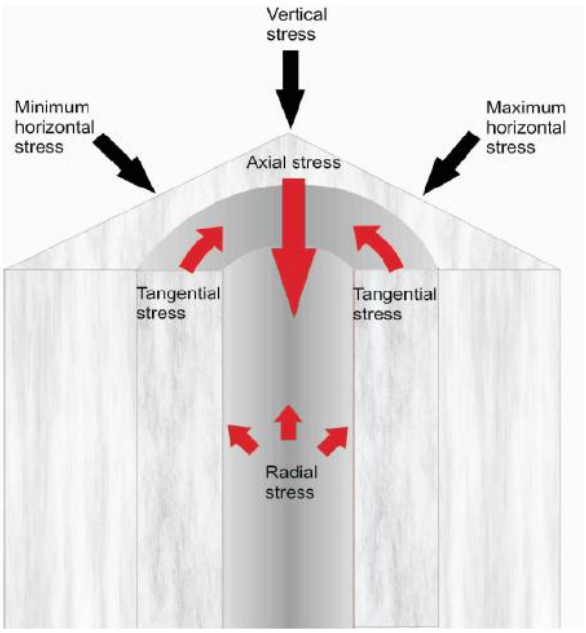

Figure 2.4: Stress distribution around a wellbore

The models vary from simple elastic models to more elaborated elastic-plastic models. Morita (2004) proposed an analytical procedure based on elasticity to evaluate the stress state around the borehole. In order to evaluate the potential for wellbore stability a realistic constitutive model must be used to compute the stresses and/or strains around the wellbore. The computed stresses and strains must then be compared against a given failure criterion. The most used shear failure criteria are Drucker-Prager, Morh-Coulomb, Modified Lade criterion (Ewy et al, 1998) or Hoek and Brown (Zang et al,2007). Tensile criterion usually consists in the comparison of the minimum effective stress to the tensile strength of the rock (Michel et al, 2010).

These models are considered very conservative, since attaining the limit stress in a point around the borehole does not necessarily imply instability. Numerical methods based on plasticity theory, such as finite difference or finite elements methods present the advantage of showing the extent of the damage region, leading to better indicator of instability. These models usually

consider two kinds of failure around the wellbore: shear failure and tensile failure. The models became more complex, as they incorporated other physical phenomenon associated with instability: poroelastic models (Detourney et al, 1993), thermoporoelastic models (Wang et al, 2003), chemo-thermoplastic model (Yu et al, 2003).

2.3.1 Orientations of breakouts and induced fractures

Schematic cross-section of a wellbore showing the orientation of breakouts and induced hydraulic and centerline fractures relative to the borehole perpendicular *in-situ* earth stress components. Broken-out or missing material is shown in dark gray. In most of the world one of the three principal stresses is oriented vertically, which requires the other two to be oriented horizontally. However, inclined stress fields do occur, especially in tectonically active areas. Breakouts form in response to the minimum and maximum stress ***components*** that are oriented perpendicular to the wellbore. Note that these components may or may not be principal stresses depending on the orientation of the wellbore relative to the *in-situ* stress field. Induced fractures tend to form perpendicular to the least principal stress; so that well-developed, borehole-parallel induced fractures form when σ3 (the minimum principal stress) is oriented perpendicularly to the borehole. Hydraulic induced fractures tend to be inclined to the wellbore when σ3 is inclined to the wellbore, although they may not form perpendicular to σ3 in this case. Imagine that Figure 1 is a cross-section of a vertical well. In a normal faulting stress regime, σmin = σ3 and σmax = σ2. In a strike-slip faulting stress regime, σmin = σ3 and σmax = σ1. In a reverse faulting stress regime, σmin = σ2 and σmax = σ1.

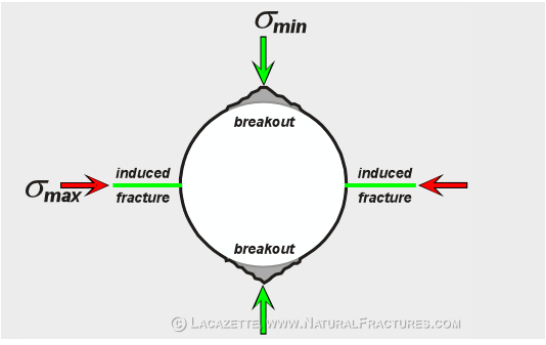

Figure 2.5: Direction of the maximum and minimum horizontal stresses

2.4 Prior Work on Wellbore Instability Modeling

Ong S. H. and J.C. Roegiers (1993) presented an anisotropic model for calculating the stress around wellbore. They concluded that the borehole collapse is a manifestation of shear failure, which in a horizontal wellbore, is significantly affected by high degrees of rock anisotropy, high in-situ stress anisotropy, and excessive cooling of the wellbore. According to Ong S. H. et al, pore pressure and porous elastic constant also affect the shear failure but the effect is less pronounced.

Morita and Ross (1993) suggested acquiring cores from vertical wells for the purpose of borehole stability analysis before drilling a highly inclined well or horizontal well. However, acquiring cores from shale intervals from a wide depth range for the purpose of borehole stability analysis could be very expensive. The application of nano-technology to drilled cutting provides a more cost effective approach to solve the problem of borehole stability while drilling.

Wong S.W., et al (1994) proposed Thick-Walled-Cylinder Strength Tests (TWC) that involved taking cores. Their method was used in deriving the necessary mechanical data used in borehole stability analysis for drilling horizontal well in North Sea. Based on their study, the elastic/brittle model prediction is unrealistically conservative. Nevertheless, the model qualitatively indicates the solution's sensitivity to different field input parameters. According to the authors, the TWC empirical approach is a new, simple method that provides a quick, qualitative borehole stability assessment. Elastoplastic analysis gives a realistic mud weight prediction, but it is the most expensive test to perform.

In 1991, lost time (Lowrey and Ottesen, 1995) due to stuck pipe related drilling problems accounted for approximately 18 % of total drilling time in Mobil Producing Nigeria (MPN) offshore operations. The primary cause of stuck pipe was identified as mechanical wellbore instability. In order to solve this problem, MPN has to carry out borehole stability study and the result was productive. Data acquisition involved taking conventional cores in the zone of interest which could make the cost of borehole stability study unattractive.

Marisela, et al (1996) used borehole stability 2-D model to analyse the borehole condition under open hole completion in Venezuela. A 2-D finite element model was developed with a generalized plasticity constitutive equation. A safe drawdown to prevent failure was determined and the well was completed open hole without any production liner. The well produced above the estimated potential without any sanding or stability problems. Cui L. and Abousleiman Y. developed 3-D model that coupled the pore fluid flow with the rock matrix. This model can be used to analyse borehole stability condition under production.

Fung L. S. K. et al (1996) also developed a finite element elasto-plastic model that can perform effective stress analysis of the near wellbore tensile and shear failure. Their model is capable of handling extremely low confining stresses in unconsolidated formation. As plastic yielding occurs at relatively low deviatoric confining stress condition, it is not a good indication of wellbore failure in terms of loss of service. They, therefore, developed a more realistic criterion based on the accumulated plastic strain. The model was successfully used to analyze the stability of two horizontal wells with open-hole completion in unconsolidated oil sand.

For modeling naturally fractured reservoirs (Zhang J. and J-C. Roegiers, 2000), the dual porosity poroelastic model is effective and accurate to characterize stresses as well as flow fields. They

developed a generalized plane strain and dual porosity finite element solution for analyzing horizontal borehole stability. Their results show that horizontal borehole stability depends strongly on the in-situ stress state, the borehole orientation, time, drilling fluid pressure and fracture characteristics.

Finkbeiner T. et al (2000) presented a case study of drilling and completing horizontal well in the shallow unconsolidated oil field of California. The evaluation of rock strength and the tectonic stress revealed that the maximum horizontal stress is greater than the overburden stress. Maximum horizontal compression is oriented $N60^{o}E$. The borehole stability of the horizontal well is predominantly controlled by the extremely weak reservoir rock. Through, the borehole stability, they predicted borehole collapse during production for open hole completion. The borehole stability analysis was also used to select the type of completion (60 mesh slotted liner) and the horizontal well produced successfully without sand problems.

Morita N. et al (2004) presented their study on "Well Orientation Effect on Borehole Stability". They came up with the following conclusions: Actual rocks are not linear elastic materials. Before a borehole collapses, the non-linearity of the rock deformation becomes significant; The significant nonlinearity reduces the stress concentration induced by directional in-situ stresses; In addition, an oriented borehole has a non-uniform stress or stress gradient around a borehole. The stress gradient reduces the stress concentration area, and the smaller size of stress concentrated region is less liable to failure due to the size effect. Wellbore remains stable after significant borehole breakouts are induced. Well stability is dominantly controlled by the maximum radial stress after local failures rather than the ratio of radial principal stresses.

Depending (Simangunsong R. A. et al, 2006) on the source of the problem, wellbore instability is classified as either mechanical or chemical. Chemical wellbore instability, often called shale instability, is most commonly associated with water adsorption in shaly formations where the water phase is present and can cause borehole collapse. In contrast, mechanical wellbore instability is caused by applying mud of insufficient weight, which will create higher hoop stresses around the hole-wall. Hoop stresses around the hole-wall are often excessively high and result in rock failure. The most rapid remedy for this instability is to increase the mud weight and/or adjust the well trajectory for high-angle wells. The mechanical instability occurs as soon as the new formation is drilled, but chemical instability is time dependent because shales are subject to strength alteration once exposed to different drilling fluids. A series of experimental studies led to the conclusion that shale strength decreases with time when the shale is exposed to most drilling fluids. Despite the tendency of shale to experience chemical instability, it can also experience mechanical instability simultaneously, which can lead to a more complex problem.

Mody F. K. et al, (2007) presented the need for a sustainable deployment of geomechanics technology to reducing well construction costs. The major hurdles in borehole stability studies currently are often due to, but not limited to, the following factors:

1. The majority of easily accessible oil and gas reservoirs have already been exploited. The trend in hydrocarbon exploration is steadily moving to deeper and more complex environments (e. g., in deep water, sub-salt HPHT and other challenging environments).

2. Data regarding rock mechanical properties, in-situ stress states and geological structures cannot be accurately defined and are often provided with large uncertainties.

3. Well engineers, petro physicists and drillers who are directly involved in well delivery may not have adequate time and training in identifying and managing borehole (in) stability issues.

4. Due to lack of resources and time constraints, well operations After Action Reviews typically gets lower priority and as a consequence these learning's may not be well documented.

Mody F. K. et al, (2007) also stated that borehole stability related downtime associated with well construction is typically 10-15 % of the total well cost and about 50 % of total non-productive time.

Drilling horizontal wells, single and multilateral, is a common practice for Saudi Aramco (Rba'a A. S. et al, 2007). For effective drilling and reservoir management, a borehole stability study was carried out to identify optimum mud weight and well azimuth to place long reach horizontal wells, so as to minimize the risk of stress-induced borehole breakouts, optimize drilling mud weights aid in making informed decision about adequate completion design, and ensure sustainable production under depletion mode. They concluded that under undepleted conditions, horizontal wells should be drilled with oil-based mud parallel to the field-derived maximum principal horizontal stress azimuth in order to maximize borehole stability and minimize required mud weights during drilling and completion.

Sinha B. K. et al (2008) presented an algorithm on how to estimate the rock stresses from borehole sonic data. Their work is only for sand reservoirs. It should be noted that most of the borehole stability problems occur in shale.

Nguyen and Abousleiman (2009) developed an analytical poro-chemo-thermo-elastic solution for an inclined wellbore that coupled transient chemical and thermal effects on shale stability.

The shale is modeled as an imperfect semi-permeable membrane which can allows partial transport of solutes. In addition to chemical osmosis, both solute transport and thermal effects are taken into account to realistically model field condition.

Furui K. et al (2009) used borehole stability analysis approach to investigate the causes of production liner deformation for inclined/horizontal wells completed in a highly compacting chalk formation. Based on the review of historical caliper survey data, they ascertain that the axial compression collapse is a major liner deformation mechanism in the reservoir zones. Axial compression collapse has been found in both low-angle wells (also build up sections horizontal wells) and horizontal laterals. The casing deformation in low-angle section are due to reservoir compaction (i.e., change in the vertical formation strain) while the deformation in horizontal sections are primarily induced by increased axial loading due to cavity deformation. The completion practice using cluster perforations and high volume acid treatments causes vertically enlarged cavities resulting in poor radial constraint.

Soreide O. K. et al (2009) study the effect of anisotropy on shale borehole stability in high pressure and high temperature well. They concluded that the effect of anisotropy is most pronounced when drilling at high inclination angles near parallel to the bedding. A mixture of failure modes may then appear.

Li S. and Purdy C. (2010) in their study on how to estimate maximum horizontal stress proposed two methods. The first method is based on a generalized Hooke's law with coupling the equilibrium of three in-situ stress components and pore pressure. They believed that this new technique can reduce the uncertainty of in-situ stress prediction by narrowing the area of the

conventional polygon of the in-situ stresses. The second method involves the analysis of drilling-induced near-wellbore stresses and breakouts by using Mohr-Coulomb failure criterion.

Lang J. et al (2011) concluded that the work flow for wellbore stability modeling should consider bedding planes, rock anisotropy and pressure depletion. With the consideration of these factors, the wellbore model enables the calculation of wellbore failures along borehole trajectories with various drilling orientations versus bedding directions.

2.5 Introduction to the Theory of Fracture Mechanics

Fracture mechanics is the field of solid mechanics that deals with the behaviour of cracked bodies subjected to stresses and strains. These can arise from primary applied loads or secondary self-equilibrating stress fields (e.g. residual stresses). The power of fracture mechanics really lies in the fact that local crack tip phenomena can, to a first order, be characterized by relatively easily measured global parameters, e.g. crack length and nominal global stress (calculated in the absence of the crack), together with finite geometry correction factors (Mustapha, 2010). Concepts in the field of fracture mechanics can be used in the failure analysis in wellbore by incorporating rock mechanical properties in to fracture mechanics models.

Fracture mechanics can be divided into linear elastic fracture mechanics (LEFM) and elastic-plastic fracture mechanics (EPFM). LEFM is applies when the nonlinear deformation of the material is confined to a small region near the crack tip (http://www.efunda.com). It assumes that the material is isotropic and linear elastic. Based on this assumption, the stress field near the crack tip is calculated using the theory of elasticity. When the stresses near the crack tip exceed the material fracture toughness, the crack will grow. For brittle materials such as rocks, it accurately establishes the criteria for catastrophic failure. In the presence of inelastic

deformation, LEFM is valid only when the size of such deformation is small compared to the size of the crack (i.e., when small scale yielding occurs) (Soboyejo, 2008).

EPFM is employed when large zone of plastic deformation develops before the crack propagates, as experienced in ductile materials. It assumes isotropic and elastic-plastic materials. Based on this assumption, the strain energy fields or opening displacement near the crack tips are calculated. When the energy or opening exceeds the critical value, the crack will grow. It should be noted that although the term elastic-plastic is commonly used in this approach, the material is merely nonlinear- elastic **(**http://www.efunda.com). In other words, the unloading curve of the so called elastic-plastic material in EPFM follows the original curve, instead of a parallel line to the linear loading part, which is normally the case for true elastic-plastic materials. This is illustrated figures below

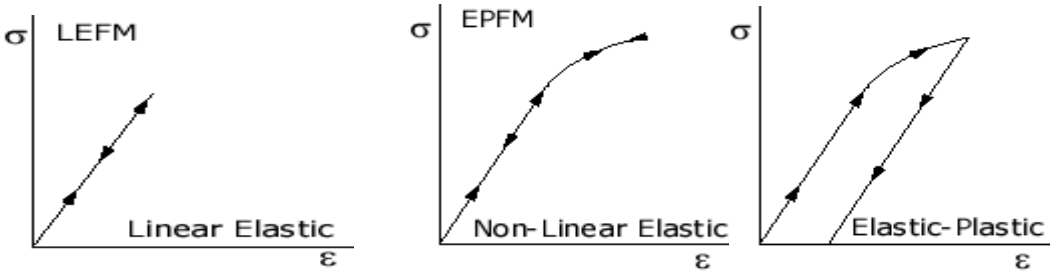

Fig 2.6: Sketches of Stress versus Strain in LEFM and EPFM (http://www.efunda.com)

2.5.1 Fracture and Modes of Fracture

Instability modeling can be considered from the point of crack propagation in the rock formation. Fracture in materials including rocks occurs in three different modes depending on the direction of failure. These are illustrated schematically in Figure. 5. Mode I [Fig. 5(a)] is generally referred to as the crack opening mode. It is often the most damaging of all the loading modes. Mode II [Fig. 5(b)] is the in-plane shear mode, while Mode III [Fig. 5(c)] corresponds to the out-

of-plane shear mode. Each of the modes may occur separately or simultaneously. Combinations of modes are referred to as mixed-mode loading (Soboyejo, 2008).

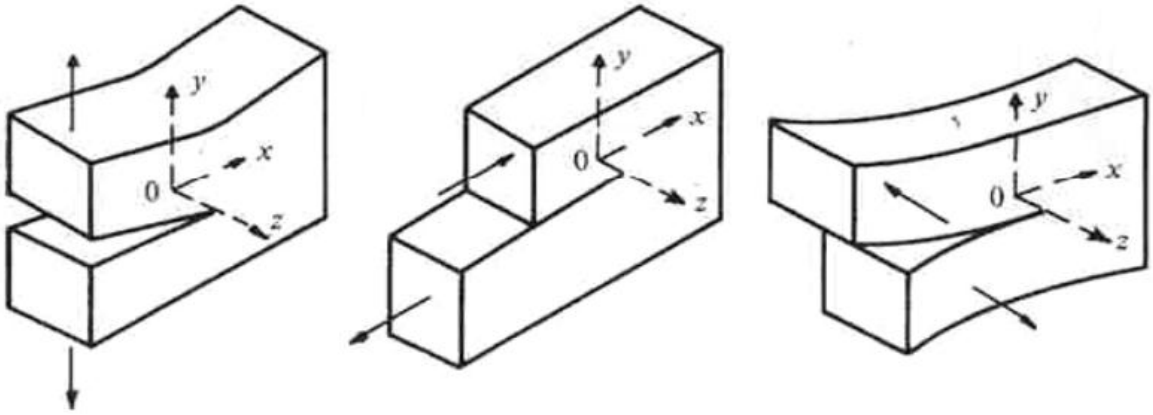

Figure 2.7: Modes of crack growth: (a) Mode I; (b) Mode II; (c) Mode III.

2.5.2 FRACTURE TOUGHNESS

During the application of fracture mechanical principles, an expression which relates the critical stress (σ_c) during crack propagation to the crack length (a) was developed. This expression is written as:

$$K_c = Y\sigma_c\sqrt{\pi a} \text{ ---------- 2.0}$$

The above expression, K_c is known as the fracture toughness or the stress intensity factor. It is a property that is a measure of a material's (rock) resistance to fracture when a crack is present. It also provides a numerical value, which quantifies the magnitude of the effect of the stress singularity at the crack tip. Fracture toughness has an unusual unit of MPa$\sqrt{m}$ or Psi$\sqrt{in}$ for oil field data (Callister, 2007).

Y is a function of the crack length (a), and width, (W). It is a dimensionless parameter that depends on the size and geometry of the specimen. It also depends on the manner in which the load is applied. This function is also known as geometry function. Geometry functions for various fracture mechanics can be found in fracture mechanics handbooks.

Since the stability of well bore structures can be determined by the growth of crack in rocks, or by the growth of interfacial crack in shale structures, a special effort will be made to study the depth dependence of rock fracture toughness and interfacial fracture toughness (Soboyejo et al 2008). The fracture toughness measurement will be performed on Chevron notched and Brazil disk specimen geometries. The Chevron notched and Brazil disk specimens will be used to measure the mode I fracture toughness levels, while the Brazil disk specimen geometry will be used to measure the mode mixity dependence on fracture toughness between pure mode I and pure mode II (Shetty D. K,1989).

Furthermore, since the International Society for Rock Mechanics (ISRM) has proposed the use of Chevron notched specimens for testing of rock fracture toughness for the core-based specimens, chevron notched specimens will be tested as controls under mode I conditions. In any case, the depth dependence of rock fracture toughness and interfacial fracture toughness will be measured for horizontal and vertical wells that are representative of those found in the Niger Delta.

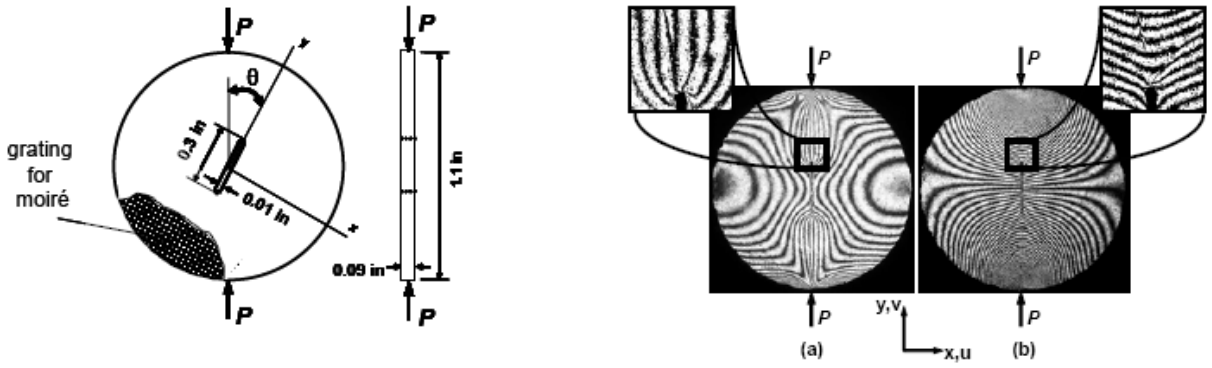

a b

Figure 2.80: Schematic description of the Brazilian disk Figure 2.81: U and V displacement fields for mode I (0°) loading.

The Brazil disk specimen Figure 6a was developed originally in 1947 to determine the fracture toughness of rocks. Early versions of the specimen were approximately 2 inches in diameter and a thickness equal to the radius. Subsequent researchers developed a "flattened" center crack disk type specimen. This newly developed specimen which was much thinner and had a pre-existing crack at the center proved to have many advantages and soon became a very popular testing tool in fracture mechanics. Since the specimen provides a wide range of mode mixity, considerable material property information can be obtained from one specimen geometry, over a range of stress states that are relevant to horizontal and vertical wells.

2.6 Nano-indentation Measurement of Mechanical Properties

Nano-indentation testing (NIT) has been developed over the past two decades. It employs high resolution electronic instrument to control and monitor loads and displacement of an indenter as it is driven into a specimen (Hay and Pharr, 2000). In this technique, small loads and tip sizes are used so indention area can be as small as few micrometers to a few nanometers. Mechanical

properties like, Young's modulus and hardness, Fracture toughness can be derived directly from load and measurements without imaging impressions (Oliver and Pharr, 2004).

Nano-indentation will be utilized initially for the measurement of the Young's moduli of rock samples that will be obtained from different depths in selected horizontal, vertical and inclined wells in the Niger Delta. The technique (Jorge Ramirez, 2010) involves the use of an indenter tip, of known geometry, in the indentation of spectra sites within a material. After loading and holding at a present maximum load, the load is reduced until complete relaxation occurs. The procedures for instrumented indentation are summarized in ASTM E2546 and ISO 14577 [www.astm.org/Standards/E2546.html]. The technique has been used to measure the elastic-plastic properties of a wide range of materials over the past few decades. Contact mechanics models have also been developed to interpret measured load-displacement data. During indentation, the load is applied by a piezo-actuator and measured in a controlled loop with a high sensitivity load cell. The position of the indenter relative to the sample surface is also precisely monitored with high precision capacitive sensor. The resulting load/displacement curves provide data specific to the deformation response of the material under examination. Established models [Jorge Ramirez, 2010] are then used to calculate hardness and modulus values for such data.

The Berkovich indenter will be utilized for Young Moduli and Rock's Hardness measurement. Multiple nano-indentations will be obtained at different depths in an effort to study the possible variations in rock mechanical properties of the oil well formation.

2.6.1 Theory of Nano-Indentation

Nano-indentation test involves indenting a specimen by a very small load using a high precision instrument, which records the load and displacement continuously. The mechanical properties of thin films coatings and substrates can be derived from the measure load-displacement loading/unloading curve through appropriate data analysis. These tests are based on new technologies that allow precise measurement and control of the indenting forces and precise measurement of the indentation depths (Agilent Technology, 2009).

In nano-indentation, a prescribed load is applied to a pyramidal or spherical indenter or other shapes in contact with the specimen surface. As load is applied to the indenter, the depth of penetration into the specimen is measured. A nano-indentation test instrument provides experimental results in the form of a load-displacement curve for the loading and the unloading parts of the indentation process as shown in Figure 2.1. An analysis of the unloading data provides a value for the depth of the circle of contact at full load. The area of contact at full load is determined from the known angle or radius of the indenter. The hardness is derived by dividing the load by the area of contact. The slope of the unloading curve provides a measure of elastic moduli (Ahmadov et al, 2009). To make accurate measurements by indentation experiments, the contact areas of the indentations must be precisely known.

2.6.2 Description of Indentation Process (Oliver and Pharr Method)

Force is applied on pyramidal shaped diamond indenter (Berkovich indenter) and indenter is forced into the specimen (Figure 2.7). This causes both elastic and plastic distortion according to the geometry of the indenter to the contact depth h_c as shown in (Figure 2.10). Topography of an indentation on fused silica is shown in Figure 2.8. When force is retracted, only elastic

component of the displacement is regained; using this 15 elastic recovery, one can calculate elastic properties, like Young's modulus and hardness of material. This technique can be applied to different types of indenter tips with axisymmetric geometries including spheres, conical and conical indenter (Oliver and Pharr, 2004). Berkovich indenter has been used in this study.

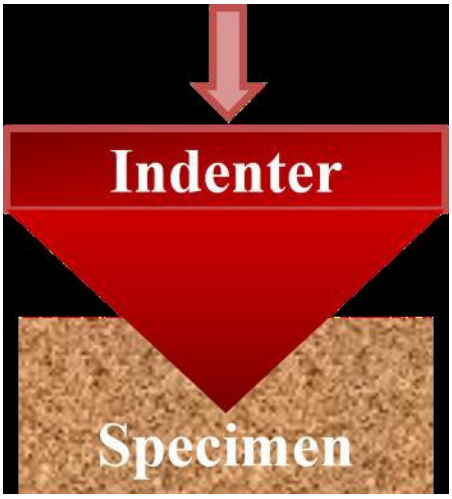

Figure 2.90: Indentation on specimen. Force in the range of mN used for the indentation.

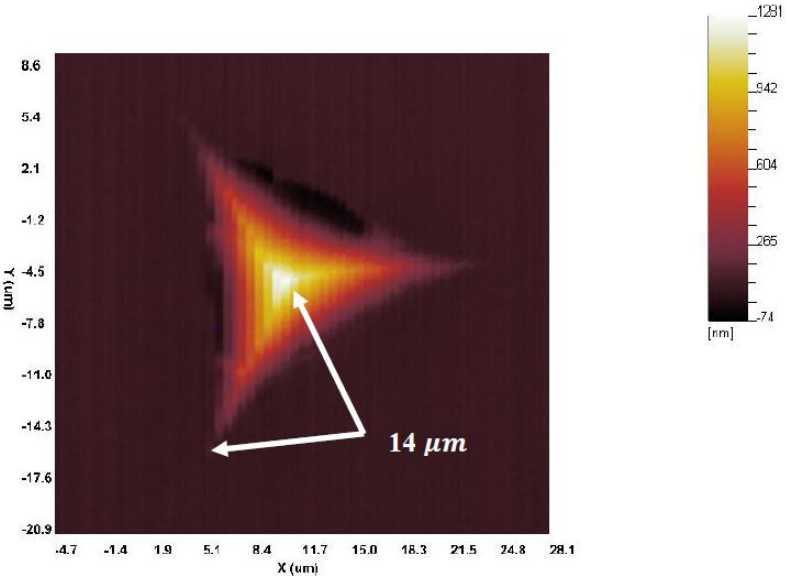

Figure 2.91: Survey scanning image of an impression on fused silica generated by nano-indenter. Radius of impression is 14 microns (Vickas, 2012)

Steps to Calculate Young's Modulus and Hardness

1. The first step in the calculation involves the generation of continuous loading and unloading data as shown in Figure 2.6. Some important parameters in the Figure 2.6 are the maximum load and displacement, P_{max} and h_{max}, the residual depth after unloading, h_f.

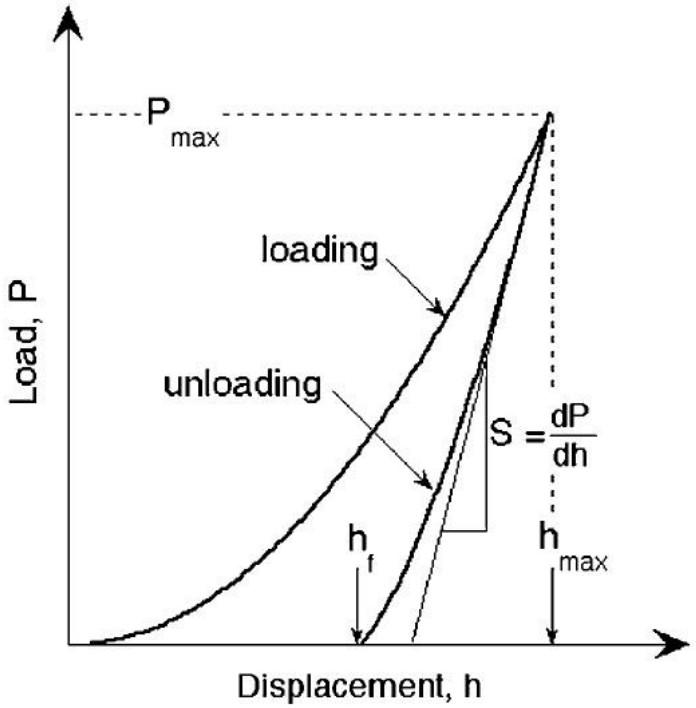

Figure 2.92: Load displacement curve during indentation process. Loading denotes the portion of increasing force on specimen, while, unloading denotes portion of decreasing force (Oliver and Pharr, 2004).

2. The second step involves approximation of unloading data by power law relationship:

$$P = \alpha(h - h_f)^m \text{---------- 2.1}$$

Where and m are power fitting constants, P is the applied load and h is the resulting penetration depth. The power law exponent (m) lies in the range of $1.2 \leq m \leq 1.6$. Generally, upper 25% of unloading data is used to determine the equation (2.1).

3. The contact stiffness, S, is determined by analytically differentiating equation (2.1) at maximum depth of penetration h = h_{max} and given by equation

$$S = \alpha m(h - h_f)^{m-1} \quad at\ h = h_{max}$$ ----------2.2

4. Fourth step involves determination of depth over which indenter remains in contact with specimen. This contact depth, h_c, is different from total penetration depth h_{max} as shown in Figure 2.6. Berkovich indenter can be modeled using conical indenter with half angle, $\emptyset = 70.3^0$. This calculation does not take into account the pile up of material occurring at the periphery of elastic-plastic matter. Assuming, pileup to be negligible, the amount of sink-in, h_s, is given by

$$h_s = \frac{\epsilon P_{max}}{S}$$ ---------- 2.3

Where is a constant and depends on the geometry of the indenter, P_{max} = maximum applied load, $S = \frac{dP}{dH}$. $\epsilon = 0.75$ for Berkovich indenter (Oliver and Pharr, 2004).

Using the equation (2.3) in Figure 10, the depth of contact, h_c, between indenter and specimen is given by

$$h_c = h_{max} - \epsilon \frac{P_{max}}{S}$$ ---------- 2.4

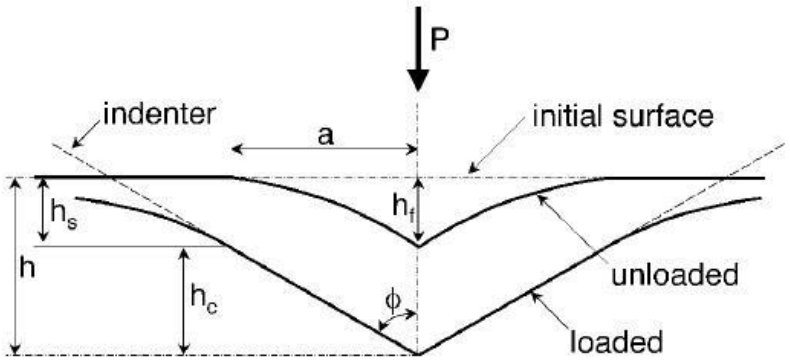

Figure 2.93: Front view of indenter impression during maximum load application and after load removal. h_f is the residual depth after unloading, h is the total depth at maximum load and $\emptyset$ is the indenter half angle. (Oliver and Pharr, 2004)

5. After calculation of contact depth hc, projected area of contact is determined by an empirically calculated area function at the depth h_c.

$$A = f(h_c)$$ ----------2.5

This area function is also called indenter shape function, which should be carefully calibrated so that departure from non-ideal geometry can be taken into consideration. These departures can be significant near the Berkovich indenter tip, where rounding happens due to grinding process during indentations after some time (Oliver and Pharr, 2004).

6. After calculation of the contact area, the hardness is calculated using following equation.

$$H = \frac{P_{max}}{A}$$ ---------- 2.6

7. Finally, measurement of the elastic modulus is done using the relationship between the contact areas and unloading stiffness using equations 2.5 and 2.7

$$S = \frac{dP}{dH} = (2 * \beta * \sqrt{A} * E^*)/(\sqrt{\pi})$$ ---------- 2.7

Where E^* is the effective elastic modulus

Equation 2.7 is a general equation applicable to any type of symmetric indenter. Originally, was taken as unity; however it was shown later that even for axisymmetric rigid cone cone indenter, it can deviate significantly from unity (Oliver and Pharr, 2004).

β= 1.034 for the Berkovich indenter. Now calculated E* is used in equation 2.8 to calculate Young's modulus, E_i, of specimen.

$$\frac{1}{E^*} = \frac{1-\gamma_i^2}{E_i} + \frac{\gamma^2}{E'}$$ ---------- 2.8

The effective elastic modulus considers the fact that displacement takes place in both the specimen, with Young's modulus E_i and poisson's ratio γ_i , and the indenter, with elastic constants and for diamond, E' = 1141GPa and γ' = 0.07 .

While it may seem counterintuitive to use Poisson's ratio to compute elastic modulus, even a rough estimate of Poisson's ratio produces little uncertainty in the elastic moduli of the most materials.

Although the nano-indenter can accommodate any indenter type, the Berkovich geometry is generally preferred for hardness and Young's modulus measurement. The Berkovich indenter is preferred because plasticity is produced at low load; it has good manufactured quality and minimizes the influence of friction.

The use of nanoindentation for determination of mechanical properties of shale was carried out by Vikas Kumar. Indentation was used to determine the mechanical properties of different shale cutting.

Shale Play	Average Ei	σ_{Ei}	Average H	σ_H
Woodford	41	12	1.4	1.3
Barnett	50	10	1.4	0.5
Haynesville	47	15	1.1	0.6
Eagle Ford	41	9	0.8	0.3
Ordovician	49	4.5	1.2	0.2
Kimmeridge	7.4	3	0.3	0.04

Table 2.0.0: Summary of average indentation Young's Modulus and average hardness with standard deviation (σ) for different shale plays (Vikas, 2012)

2.7 Finite Element Analysis

The measurements of Young's Moduli, compressive strength and fracture toughness will be incorporated into finite element models of wellbore structures. The models, which will be developed within commercial software package ABAQUS CAE 6.12 (teaching edition), will include formation layers within actual properties obtained from the indentation and fracture toughness experiments. The initial simulation will explore the effect of hydrostatic pressure due to drilling operations. The underlying rock stress distributions and crack driving forces will be computed for the layered structure under well controlled hydrostatic stress conditions. The program will then apply conventional Mohr-Coulomb criteria and fracture mechanics approaches to the determination of critical conditions for well bore instability and hence the drilling fluid window for optimal drilling and production operations. The insights from these simulations will be used to develop guidelines for the use of indentation and fracture mechanics properties in the design of well bore stability in horizontal and vertical wells in the Niger Delta.

REFERENCES

http//:www.astm.org/Standards/E2546.htm

Abousleiman, Y., Kanj, M., Ekbote, S., 2001. Poromechanical Tools for Reservoir Rock Testing Simulation and Wellbore Stability. Paper presented at the SPE Annual Technical Conference and Exhibition held in New Orlean, Lousiana, U.S.A.. SPE 71459.

Agilent Technologies. 2009. G200 User's guide. Chandler, Arizona, USA.

Ahmadov, R., Vanorio, T. and Mavko, G. 2009. Confocal Laser Scanning and Atomic Force Microscopy in Estimation of Elastic Properties of the Organic Rich Bezhenov Formation. *The Leading Edge*, **28** (1): 18-23.

Chatterjee, R., Mukhopadhyway, M., 2003. Numerical Modeling of Stress Around a Wellbore. Paper presented at the SPE Asia Pacific Oil and Gas Conference and Exhibition held in Jakarta, Indonesia. SPE 80489.

Cul, L., Abousleiman, Ekbote, S., Roegiers, J-C., Zaman, M., 1999. A Software for Poroelastic Analyses of Borehole Stability. Paper presented at the SPE Latin American and Caribean Petroleum Engineering Conference held in Caracas, Venezuela. SPE 54013.

Detournay, E. and Cheng, A.H-D, Fundamentals of poroelasticity, Chapter 5 in Comprehensive Rock Engineering: Principles, Practice and Projects, Vol. II, Analysis and Design Method: 113-171, ed. C. Fairhurst, Pergamon Press, 1993.

Ewy, R.T., Wellbore Stability Predictions Usina a Modified Lade Criterion. SPE Eurorok 98,

Finkbeiner, T., Moos, D., DeRose, W., Shiflet, D., 2000. Wellbore Stability Evaluation for Horizontal Completion – A Case Study. Paper presented at the SPE Asia Pacific Oil and Gas Conference and Exhibition held in Brisbane, Australia. SPE 64409.

Fontana, H., Paris, M., Ong, Seehong., 2007. Borehole Stability (Geomechanics) Modeling and Drilling Optimization Practices Improve Drilling Curves in Naturally Fractured Shale – A South Argentina Experience. Paper presented at the SPE/IADC Middle East Drilling Technology Conference and Exhibition held in Cairo, Egypt. SPE/IADC 107474.

Fuh, G-F., Deom, D. B., Turner, R. D., 1991. Wellbore Stability and Drilling Results From the First Horizontal Well in the Kotter Field Offshore The Netherlands. Paper presented at the 66th Annual Technical Conference and Exhibition of the Society of Petroleum Engineers held in Dallas, TX. U.S.A. SPE 22544.

Fung, L. S. K., Wan, R. G., Rodriguez, H., 1999. An Advanced Elasto-plastic Model for Borehole Stability Analysis of Horizontal Wells in Unconsolidated Formation. Paper presented at the 47th Annual Technical Meeting of The Petroleum Society in Calgary, Alberta, Canada. PAPER 96-58.

Furul, K., Fuh, G-F., Abdelmalek, N., 2009. Acomprehensive Modeling Analysis of Borehole Stability and Production Liner Deformation for Inclined/Horizontal Wells Completed in a Highly Compacting Chalk Formation. Paper presented at the SPE Annual Technical Conference and Exhibition held in New Orlean, Lousiana, USA. SPE 123651.

Furul, K., Fuh, G-F., Abdelmalek, N., 2010. Acomprehensive Modeling Analysis of Borehole Stability and Production Liner Deformation for Inclined/Horizontal Wells Completed in a Highly Compacting Chalk Formation. Drilling and Completion. SPE 123651.

Gaurina-Međimurec, N. (1994): Mechanical Factors of Wellbore Instability, Nafta 45 (3), Zagreb. Geothecnical and Geoenvironment Engineering, 113: 1128-1135, 2007.

Jorge Ramirez; 2010. (www.nanovea.com/nanofracturetoughness.pdf)

Lang, J., Li, S., Zhang, J., 2011. Wellbore Stability and Real-Time Surveillance for Deepwater Drilling to Weak Bedding Planes and Depleted Reservoirs. Paper presented at the SPE/IADC Drilling Conference and Exhibition held in Amsterthan, The Netherlands. SPE 139708.

Lang, J., Li, S., Zhang, J., 2011. Wellbore Stability and Real-Time Surveillance for Deepwater Drilling to Weak Bedding Planes and Depleted Reservoirs. Paper presented at the SPE/IADC Drilling Conference and Exhibition held in Amsterthan, The Netherlands. SPE 139708.

Li, S., Purdy, C., 2010. Maximum Horizontal Stress and Wellbore Stability White Drilling: Modeling and Case Study. Paper presented at the SPE Latin American and Caribean Petroleum Engineering Conference held in Lima Peru. SPE 139280.

Lowrey, J. P., Ottesen, S., 1995. An Assessment of the Mechanical Stability of Wells Offshore Nigeria. SPE Drilling and Completion.

Marisela, S. D., Cabrera, S., Jose, R. 1996. Geomechanical Design and Evaluation of a Horizontal Wellbore in Maracaibo Lake, Venezuela: Real-Drilling-Time Application. Paper presented at the SPE International Conference held in Calgary, Canada. SPE 37088.

Martins, A.L., Santana, M.L., Goncalves, C.J.C., Gaspari, E., Campos, W., Perez, J.C.L.V. (1999): Evaluating the Transport of Solids Generated by Shale Instabilities in ERW Drilling Part II: Case Studies, paper SPE 56560 presented at the 1999 SPE annual Technical Conference and Exhibition, 3-6 October, Houston, Texas.

McLean, M.R. Addis, M.A. (1990): Wellbore Stability Analysis: A Review of Current Methods of Analysis and Their Field Application, paper IADC/SPE 19941 presented at the 1990 IADC/SPE Drilling Conference, 27 February - 2 March, Houston, Texas.

Mody, F. K., Tare, U., Wang, G. G., 2008. Application of Geomechanics Technology in Borehole Stability Reduces Well Construction Costs. Paper presented at San Francisco 42nd US Rock Mechanics Symposium and 2nd US-Canada Rock Mechanics Symposium held in San Francisco. ARMA 08-255.

Mody, F. K., Tare, U., Wang, G., 2007. Sustainable Deployment of Geomechanics Technology to Reducing Well Construction Costs. Paper presented at the SPE/IADC Middle East Drilling Technology Conference and Exhibition held in Cairo, Egypt. SPE/IADC 108241.

Mody, F.K. and Hale, AH.: "A Borehole Stability Model to Couple The Mechanics and Chemistry of Drilling Fluid Interaction," Proc. SPIVIADC Drilling ConJ, 1993, 473-490. Amsterdam, The Northlands.

Morita, N., 2004. Well Orientation Effect on Borehole Stability. Paper presented at the Annual Technical Conference and Exhibition held in Houston Texas U.S.A. SPE 89896.

Morita, N., Ross, C. K., 1993. Core-Based Horizontal or highly Inclined Well Stability Analysis for Unconsolidated Formations. Paper presented at the 68th Annual Technical Conference and Exhibition of the Society of Petroleum Engineers held in Houston, TX. U.S.A. SPE 26332.

Mustapha K., 2010. Strength and Fracture of Earth-Based and Natural Fibre-Reinforced Composite. Unpublished Thesis Submitted to the Graduate Faculty, African University of Science and Technology, Abuja.

Nguyen, V. X., Abousleiman, Y., 2009. The Porochemothermoelastic Coupled Solutions of Stress and Pressure with Applications to Wellbore Stability in Chemically Active Shale. Paper presented at the SPE Annual Technical Conference and Exhibition held in New Orlean, Lousiana, USA. SPE 124422.

Oliver, W.C., and Pharr,G.M. 2004. Measurement of Hardness and Elastic Modulus by Instrumented Indentation: Advances in Understanding and Refinements to Technology. *J. Mater. Res.* **19**(1): 3-20.

Ong, S. H., Roegiers, J-C., 1993. Horizontal Wellbore Collapse in an Anisotropic Formation. Paper presented at the Productions Symposium held in Oklahoma City, OK. U.S.A. SPE 25504.

Potter, E. P, Maynard, J. B., Pryer, W. A.: Sedimentology of Shale, Springer-Verlag, N. Y., 1984.

Raba'a, A. S., Abass, H. H., Hembling, D. E., 2007. A geomechanical Facies-Based Approach To Optimize Drilling and Completion Strategy of an Unconsolidated Sandstone Reservoir, Saudi Arabia. Paper presented at the SPE Annual Technical Conference and Exhibition held in Anaiheim, Califonia, U. S. A. SPE 109774.

Shetty, D. K., Fracture Toughness of Polycrystalline Ceramics in Combined Mode I and Mode II Loading, *J. Am. Ceram.Soc.*, (1989)

Simangunsong, R. A., Villatoro, J. J., Davis, A. K., 2006. Wellbore Stability Assessment for Highly Inclined Wells Using Limited Rock-Mechanics Data. Paper presented at the SPE Annual Technical Conference and Exhibition held in San Antonio, Texas, U. S. A.. SPE 99644.

Sinha, K. B., Wang, J., Kisra, S., Li, J., Pistre, V. Bratton, T., Sanders, M., 2008. Estimation of Formation Stresses Using Borehole Sonic Data. Paper presented at the SPWLA 49th Annual Logging Symposium held in Edinburgh, Scotland.

Soreide, O. K., Bostrom, B., Horsrud, P., 2009. Borehole stability simulation of an HPHT field using anisotropic shale modeling. Paper presented at Asheville 43rd US Rock Mechanics Symposium and 4th US-Canada Rock Mechanics Symposium held in Asheville. ARMA 09-185.

Tare, U. T., Mody, K. F., Mese, A. I., 2000. Understanding Chemical-Potential-Related Transient Pore-Pressure Response To Improve Real-Time Borehole (In)Stability Predictions. Paper presented at SPE/Petroleum Society of CIM International Conference on Horizontal Well Technology held in Calgary, Alberta, Canada. CIM 65514. Trondhelm, Nonway, 08-10 July 1998.

Vikas K., 2012. Geomechanical Characterization of Shale Using Nano-indentation. Unpublished thesis submitted at the Mewbourne School of PetroleumAND Geological Engineering, University of Oaklahoma, USA.

Wang Y.1; Dusseault M.B. A coupled conductive-convective thermo-poroelastic solution and implications for wellbore stability. Journal of Petroleum Science and Engineering, Volume 38: 187-198, 2003.

Wole Soboyejo, Mechanical Properties of Engineered Materials,2008

Wong, S-W., Veeken, C. A. M., Kenter, C. J., 1994. The Rock-Mechanical Aspects of Drilling and North Sea Horizontal Well. SPE Drilling and Completion.

Yu, M, Chevernet, M.E., Sharma, M.M., Chemical–mechanical wellbore instability model for shales : accounting for solution diffusion. Journal of Petroleum Science and Engineering, 38:131-143, 2003.

Zang, L., Zhu, H., Three-Dimensional Hoek-Brown Strength Criterion for Rocks. Journal of

Zhang, J., Roegiers, J-C., 2000. Horizontal Borehole Stability in Naturally Fractured Reservoirs. Paper presented at the SPE/The Petroleum Society of CIM International Conference on Horizontal Well Technology held in Calgary, Alberta, Canada. CIM 65513.

Zhou, X. X., Ghassemi, A., 2008. Chemo-poromechanical Finite Element Modeling of a Wellbore in Swelling Shale. Paper presented at San Francisco 42nd US Rock Mechanics Symposium and 2nd US-Canada Rock Mechanics Symposium held in San Francisco. ARMA 08-161.

Chapter 3

3.0 Analytical and Computational Modelling of Wellbore

3.1 Introduction

Oil wells are made of shale formation of varying composition that occurs in layers has one go down the well. In order to understand the failure mechanism during drilling, concepts from fracture mechanics provide insight into the underlying cause of failure during drilling. In this chapter, wellbore stability problem during drilling was modeled analytically with consideration of cracks within a formation and between the shale formations. The Critical conditions for unstable crack growth are determined by equating numerical finite elements of crack driving forces to the published fracture toughness data for shale cracks. The predicted upper mud weights pressures are also compared with results are elucidated for the determination of the upper pressure ranges during drilling operations.

3.2 Crack Modeling within a Formation Layer

For Crack within a layer of shale formation can be described mathematically by considering a crack of length 2a in the region of a nominal far field stress of. The mode I stress intensity factor is given by (Swamy, 1979):

$$K_1 = Y\sigma\sqrt{\pi a} \quad \text{---------- 3.0}$$

Where Y is a non-dimensional function depending on the size and geometry of the crack

If an oil well is loaded to failure stress σ_f , then the value of the nominal far field stress at the onset of failure can be associated with the critical fracture toughness,K_{IC}, for cracks within the

shale. Hence, for simple crack formations within the shale structure σ_f can be obtained by rearranging equation 3.0 to give:

$$\sigma_f = \frac{K_{IC}}{Y\sqrt{\pi a}} \text{ ---------- 3.1}$$

The critical stress intensity factor, K_{IC}, unstable crack growth may also be expressed in terms of the energy release rate, G (Bocca et al, 1991). These are related through the following expression (Barsom et al, 1987).

$$G_I = \frac{K_I^2}{E'} \text{ ---------- 3.2}$$

E' = E (for plane stress condition) ----------3.3a

$E' = \frac{E}{1-v^2}$ (for plane strain condition)----------3.3b

Furthermore, in general for mixed mode loading conditions, the energy release rate is a scalar quantity. Hence, for combined modes I, II and III, the energy release rate and stress intensity factors are given by:

$$G = G_I + G_{II} + G_{III} = \frac{(K_I^2 + K_{II}^2) + (1+v)K_{II}^2}{E'} \text{----------3.4}$$

3.3 Interfacial Crack Modeling In Shale Formation

In brittle materials such as shale formations in oil wells, and crack growth is controlled by the crack driving forces and mode mixity levels (cottrel and Rice, 1980; Evans et al, 1999). Fracture at the interface is more complex, since crack-tip fields exhibit an oscillating singularity (Soboyejo, 2008). Nevertheless the crack driving forces and mode mixity levels can be computed

using basic principles in interfacial fracture mechanics. For interfacial crack in a half space, the amplitude of the normal and shear stresses at a distance, x, ahead of a plane strain interfacial crack are characterized by two stress intensity factors, K_I and K_{II} (Soboyejo, 2008). These are given by

$$\sigma_{22} = \frac{K_I}{\sqrt{2\pi x}} \text{ ---------- 3.5a}$$

$$\sigma_{12} = \frac{K_{II}}{\sqrt{2\pi x}} \text{ ---------- 3.5b}$$

σ_{22} and σ_{12} can be calculated using Finite Element Method However, in this case the crack-tip field exhibits an oscillating singularity. Furthermore, the crack driving forces can be computed using the path dependent J integral, which may be obtained from finite element analyses in which the paths are selected to be outside the region of oscillating singularity (Soboyejo,2008). Furthermore, for the interfacial crack, the critical cracking condition and the crack paths are both affected by the mode mixity, ψ, which defined as

$$\Psi = tan^{-1}\left(\frac{k_I}{K_{II}}\right) \text{----------3.6a}$$

The mode mixity can also be expressed in terms of the energy release rate G, given by

$$\Psi = tan^{-1}\left(\frac{G_I}{G_{II}}\right) \text{----------3.6b}$$

In any case, the conditions for interfacial failure in shale formations will correspond to the conditions at which the combined energy release rate at the particular mode mixity.

In the case of interfacial crack, the effective G is given by the average of G_I and G_{II}

$$J = G = \frac{1}{2}(G_I + G_{II}) \text{----------3.7}$$

$$J = \frac{1}{2}\left(\frac{1-v_1^2}{E_1} + \frac{1-v_2^2}{E_2}\right)(k_I^2 + k_{II}^2)$$ ----------3.8

$$J_c = \frac{1}{2}\left(\frac{1-v_1^2}{E_1} + \frac{1-v_2^2}{E_2}\right)(K_{IC}^2 + K_{IIC}^2)$$----------3.9

Where the subscripts I and II denotes modes I and II and the subscript 1 and 2 denotes the two dissimilar rock formations and J_C is the critical J-integral.

3.4. Finite Element Simulation

Finite Element Analysis (FEA) provides a reliable numerical technique for analyzing engineering designs. The process starts with the creation of a geometric model. Then, the program subdivides the model into small pieces of simple shapes called elements connected at common points called nodes. The process of subdividing the model into small pieces is called meshing. Finite element analysis programs look at the model as a network of interconnected elements**.**

3.4.0. Boundary Condition and Symmetry

The model consist of a single layer of shale layer for crack within a layer as shown in fig. below and two layers of for interfacial crack. Due to symmetry of geometry of crack within a layer, one fourth of the wellbore was modeled as shown in fig. below. The model was constrained in the x and y axes to capture the true nature of an oil well. For the purpose of simplicity, longitudinal section of an oil well was modeled for interfacial crack as shown in the fig. below. Due to symmetry, half of the geometry was modeled as shown in fig.3.0.0 – 3.0.1. The model was constrained in the x and y axis respectively.

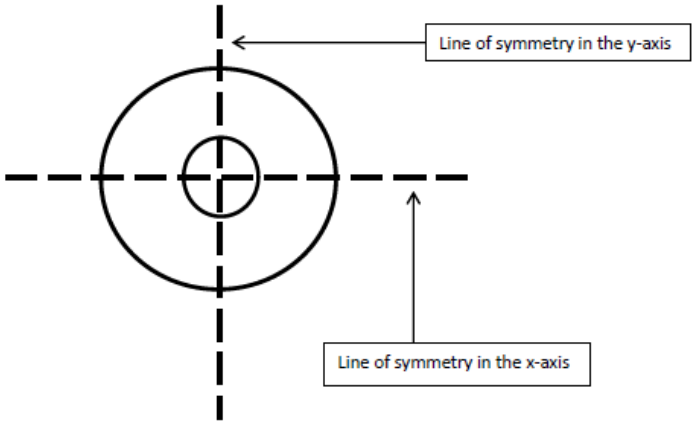

Figure. 3.0.0: Transverse section of well model showing symmetry

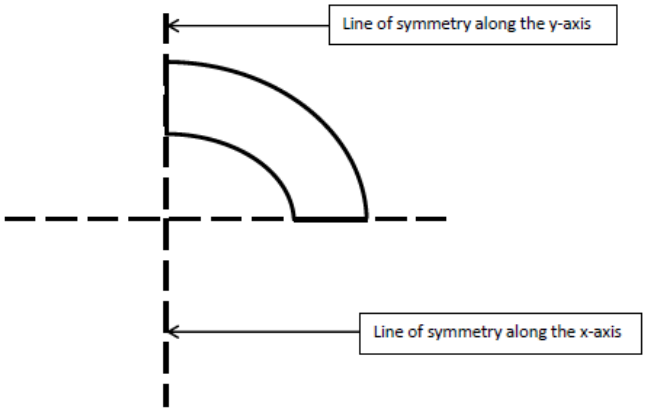

Figure. 3.0.1: Transverse section showing one fourth of the wellbore

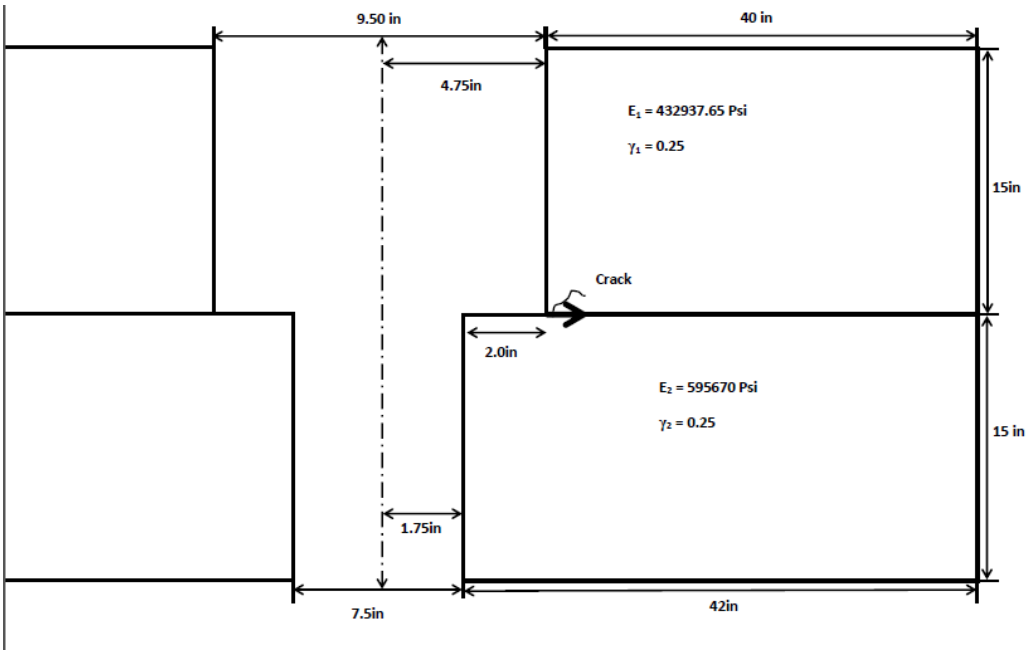

Figure 3.0.2: Longitudinal section of oil well showing the interface between two layers

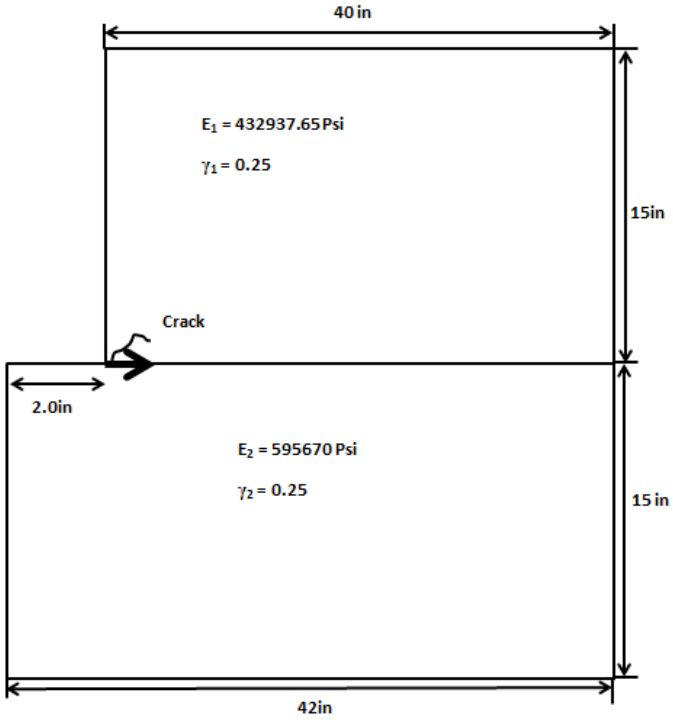

Figure 3.0.3: Longitudinal section of one half the well for interfacial crack

3.4.1 Meshing and Type of Mesh Used

Meshing is done in stages as a step-by-step development. The region where crack was applied was meshed more finely and the mesh was biased towards the tip of the crack for the purpose of accuracy during analysis. Quad structured 4-noded solid element was used for meshing. The model was analyzed using plane strain conditions.

3.5 Model Validation Using Strength Based Failure Criterion

For idealization in which the effects of cracking are not considered, tensile failure occurs when the stress imposed by drilling mud exceeds the tensile strength of the formation. The extremely excessive weight of drilling mud can create hydraulic fracture, which triggers massive circulation loss and matrix deformation. The mud weight generated using fracture mechanics model presented above will be compared to value predicted by with a simple tensile failure criterion (Simangunsong et al., 2006; Zhang et al, 2006). This gives:

$$\sigma_h - P_r \leq \sigma_{tensile} \text{ ---------- 3.10}$$

Where σ_h the minimum horizontal is stress and P_r is the pore pressure. These can both be obtained from field data. However, in the case of the minimum horizontal stress, it can also be estimated from finite element simulations or by idealization of the wall with a thick walled cylinder model (Wong et al, 1994).

3.6 Lame's Model for a Thick Wall Cylinder

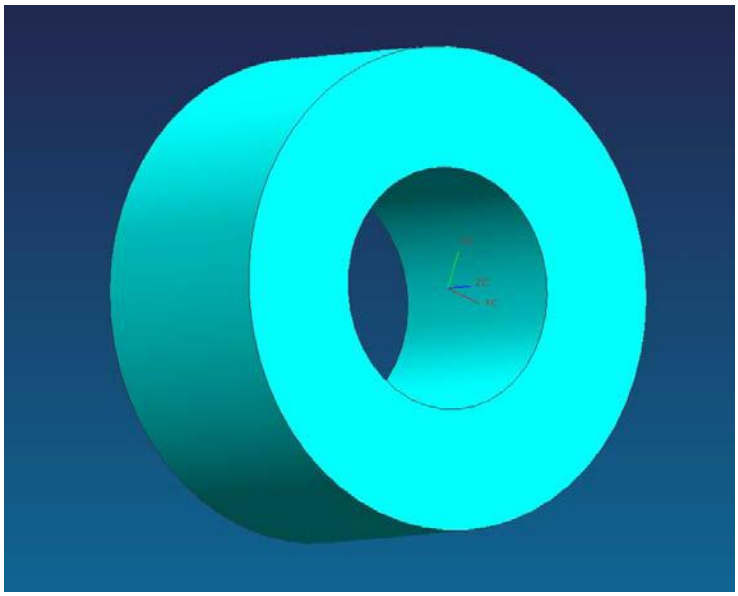

Figure.3.0.4: Thick walled cylinder with open ends

The pressure loading of a wellbore can be idealized by the classical Lame problem for a thick walled cylinder (figure 3.0.0 and 3.0.1). This gives the hoop and radial stresses respectively are expressed in terms of the internal and external radius respectively.

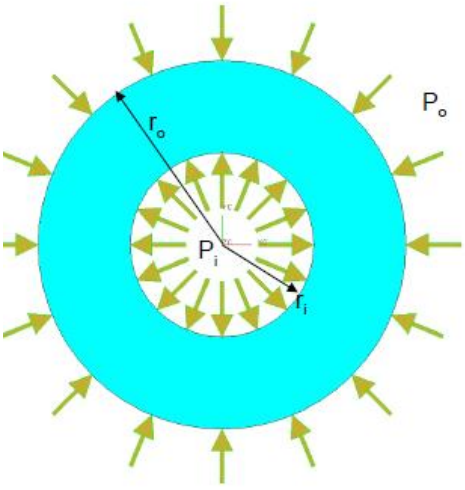

Figure.3.0.5: Cross section of thick walled cylinder loaded by internal pressure

Where r_i is the inner radius, r_o is the outer radius, P_i is the pressure on the inner face and P_o is the pressure on the outer surface.

$$\sigma_r = \frac{r_i^2 P_i - r_o^2 P_o}{r_o^2 - r_i^2} - \frac{(P_i - P_o) r_i^2}{(r_o^2 - r_i^2) r^2} \text{----------3.11a}$$

$$\sigma_\theta = \frac{r_i^2 P_i^2 - r_o^2 P_o}{r_o^2 - r_i^2} + \frac{(P_i - P_o) r_i^2 r_o^2}{(r_o^2 - r_i^2) r^2} \text{----------3.11b}$$

For the idealization of pressure loading of a wellbore, the external pressure is zero. Under this condition, the stress equations are reduced to:

$$\sigma_\theta = \frac{P_i r_i^2}{r_o^2 - r_i^2}\left[1 - \frac{r_o^2}{r^2}\right] \text{----------3.2a}$$

$$\sigma_r = \frac{P_i r_i^2}{r_o^2 - r_i^2}\left[1 + \frac{r_o^2}{r^2}\right] \text{----------3.2b}$$

$$\sigma_z = \frac{P_i r_i^2}{r_o^2 - r_i^2} \text{----------3.2c}$$

Where σ_θ is the circumferential or tangential stress (a positive value is a tensile stress), σ_r is the radial stress (a positive value is a compressive stress) and σ_z is the axial stress and is assumed to be zero for easy computation.

REFERENCES

Cottrell, A.H. (1961) Iron and Steel Institute. Special Report. vol. 69, p 281.

Evans, A.G., Hutchinson, J.W., and Wei, Y. (1999) Acta mater vol. 113, p 4093.

Rice, J.R., Drugan, W.J., and Sham, T.-L. (1980) Elastic–plastic analysis of growing cracks. In: Fracture mechanics, 12th Conference. Special Technical Publication 700, ASTM, Conshocken, PA, pp 189–221.

Simangunsong, R.A., Villatoro, J.J., Davis, A.K. (2006): Wellbore Stability Assessment for Highly Inclined Wells Using Limited Rock-Mechanics Data, paper SPE 99644 presented at the 2006 SPE Annual Technical Conference and Exhibition, 24-27 September, San Antonio, Texas, U.S.A.

Wole Soboyejo, Mechanical Properties of Engineered Materials, 2008.

Wong, S-W., Veeken, C. A. M., Kenter, C. J., 1994. The Rock-Mechanical Aspects of Drilling and North Sea Horizontal Well. SPE Drilling and Completion.

Zhang, J., Yu, M., Al-Bazali, T.M., Ong, S., Chenevert, M.E., Sharma, M.M., Clarc, D.E. (2006): Maintaining the Stability of Deviated and Horizontal Wells: Effects of Mechanical, Chemical, and Thermal Phenomena on Well Designs, paper SPE 100202, presented at the 2006 SPE International Oil & Gas Conference and Ehibition in China in Beijing, China, 5-7 December.

Chapter 4

4.0 Results and Discussion

4.1 ABAQUS Simulation of Crack Within a Layer of Shale

The rock mechanical properties of shale of an oil well obtained from the Niger Delta region of Nigeria was incorporated into $ABAQUS^{®}\ CAE\ 6.12$ (teaching edition). The wellbore stability of the well was simulated using Young's Modulus of 1.24Psi and internal wellbore diameter of 9.5in as reported in an oil field data in 2011. The external diameter was 60in for near wellbore analysis. The analysis was carried out at crack lengths of 0.2, 0.4, 0.6 and 0.8in respectively. The fracture toughness of the shale formation used was 818.89Psi-in*1/2 (Fisher, 1994) with a Poisson ratio of 0.25 (oil field data, 2011).

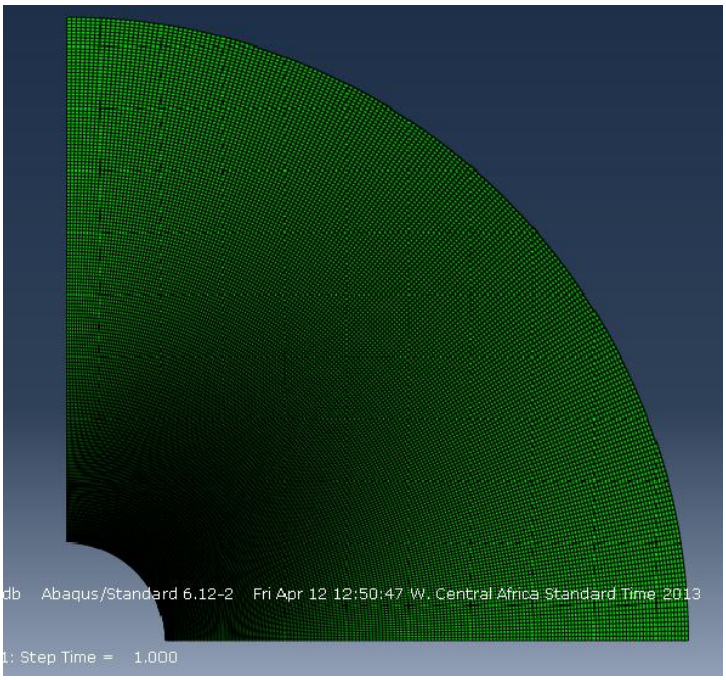

Figure 4.0.0: Wellbore Model before deformation within formation layer

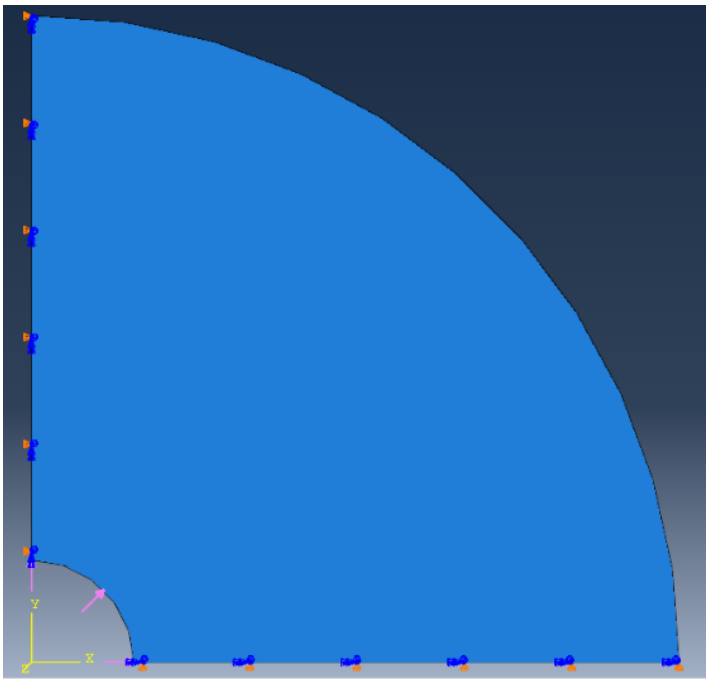

Figure 4.0.1: Wellbore Model showing point of pressure application for drilling

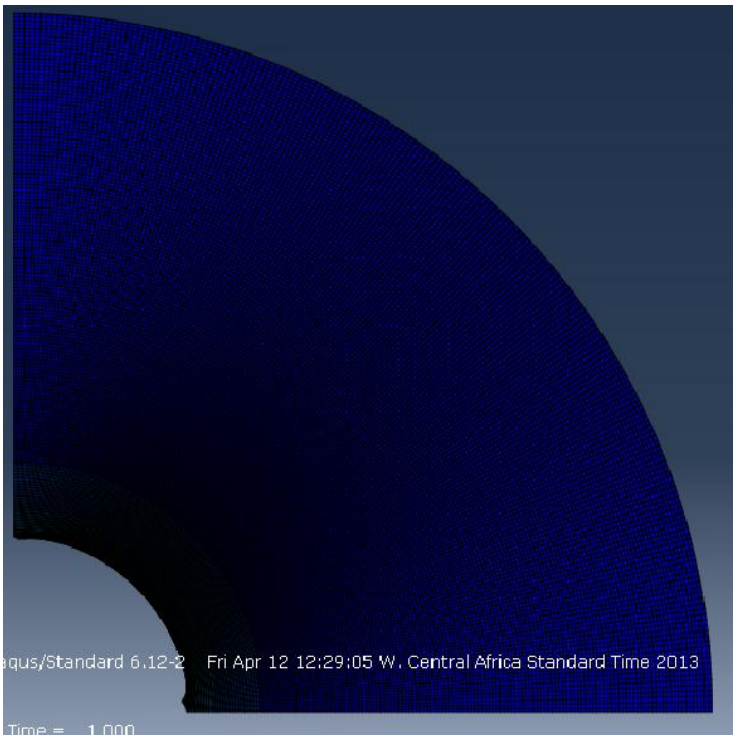

Figure. 4.0.2: Wellbore model after deformation

4.2 Stress Intensity Factor Estimate

The stress intensity factor of the layer of different crack lengths was obtained from Finite Element Simulation using $ABAQUS^{®}$ 6.12 (teaching version). Table.4.0 summarizes the stress intensity factors of the rock formation at different crack lengths.

Table 4.0.0 : Fracture toughness-Pressure data at different crack length

Pressure (Psi)	K_1 at 0.2in Crack length	K_1 at 0.4in Crack length	K_1 at 0.6in Crack length	K_1 at 0.8in Crack length
6205.36	223.154	416.365	1017.6	3629.54
6458.64	455.416	849.724	2076.73	7407.22
6711.92	696.787	1300.08	3177.4	11333
6965.2	947.266	1767.43	4319.6	15407
7218.48	1206.85	2753.11	5503.34	19629.1
7471.76	1475.55	3271.44	6728.61	23999.4
7725.04	1753.35	3806.76	7995.41	28517.8
7978.32	2040.27	3806.76	9303.75	33184.3
8231.6	2336.29	4376.08	10653.6	37999
8484.88	2641.42	4928.4	12045	42961.8

4.3 Determination of Upper Bound Mud Weight Pressure for Drilling

The pressure of the mud for drilling is an important parameter that Petroleum Engineers are concern about during drilling. The choice of the drilling pressure determines to a large extent the stability of the wellbore during drilling and production. Data generated from the finite element modeling the oil well and considering crack in a layer of shale allows for the optimum drilling

pressure at different crack lengths. Plots of stress intensity factor against pressure follow by interpolation at the fracture toughness value of the shale formation gives the corresponding pressure for drilling. Above this pressure the formation fails by fracture. Table 4.0.1 gives the drilling pressure at different crack length for a given oil well in the Niger Delta region.

Also, a plot of stress intensity factors against pressure was generated, as shown in figure 4.0. This implies that the stress distribution around the crack region is increases as the crack in the layer grows. It becomes important to consider the crack length during simulation to determine the upper bound mud weight drilling pressure.

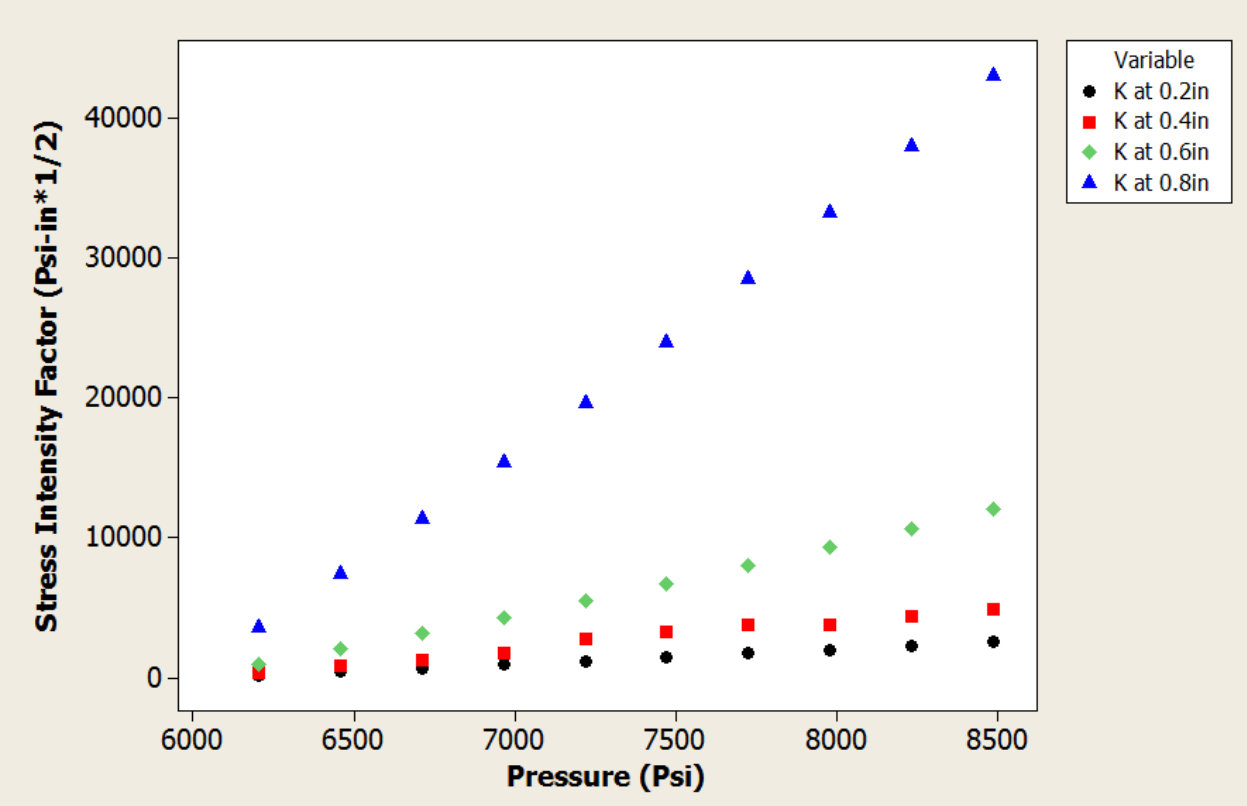

Figure 4.0.3 : Plot of Stress Intensity Factor Versus Pressure (Obtained for Different Crack Lengths)

4.4 Effect of Increase in Crack Length on the Drilling Pressure

The critical drilling pressures obtained by equating the crack driving force to the fracture toughness, K_{IC}, presented in the Fig.4.0.4. As the crack length increases, the critical drilling pressure reduces. This implies that the failure stress becomes lower and the formation can fail easily. Table 4.0.1 and fig.4.0.4 show the relationship between the critical drilling pressure and the cracklength, for cracks within the shale structure. In the case of interfacial cracks, the critical crack lengths were estimated by equating the energy release rate to the critical rate, G_C. The results are shown in fig.4.0.9 and table 4.0.4.

Table 4.0.1: Upper Bound Mud Weight Drilling Pressure - Crack Length Data

Upper Bound Mud Weigth Drilling Pressure (Psi)	Crack Length (in)
6819.56	0.2
6418.00	0.4
6217.69	0.6
6096.33	0.8

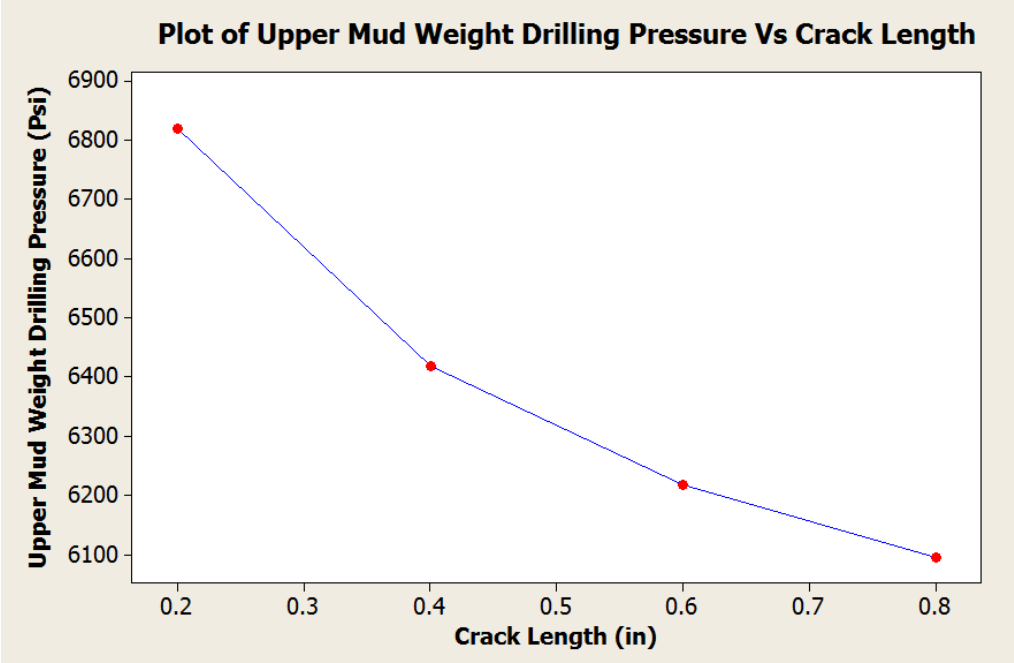

Figure 4.0.4: Plot of Drilling Pressure against Crack Length

4.5 Interfacial Crack Modeling and Simulation

Interfacial crack was modelled between two layers of shale of different materials properties. The mechanical poperties of the shale layers is shown the table below:

Table 4.0.2: Materials Properties of ShaleI and ShaleII

Materials Property	Shale I	Shale II
Young's Modulus (Psi)	432937.65	595670
Poisson Ratio	0.25	0.25
K_{IC} (Psi-in*1/2)	818.89	818.89
K_{IIC} (Psi-in*1/2)	2-3 of K_{IC}	2-3 of K_{IC}

Figure4.0.5: Undeformed Shale Layer with Crack

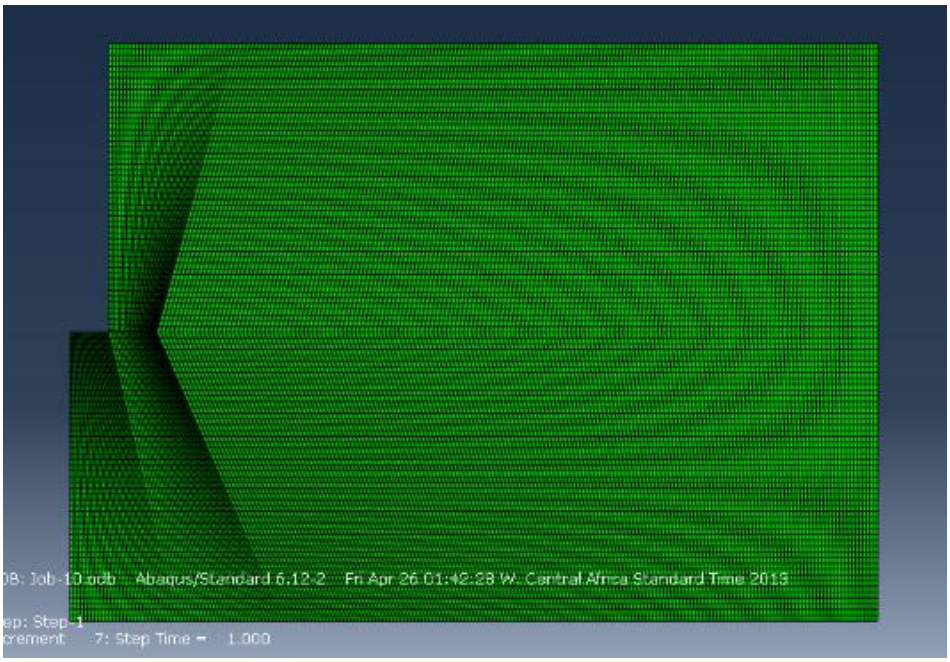

Figure4.0.6: Meshed Oil Well Model

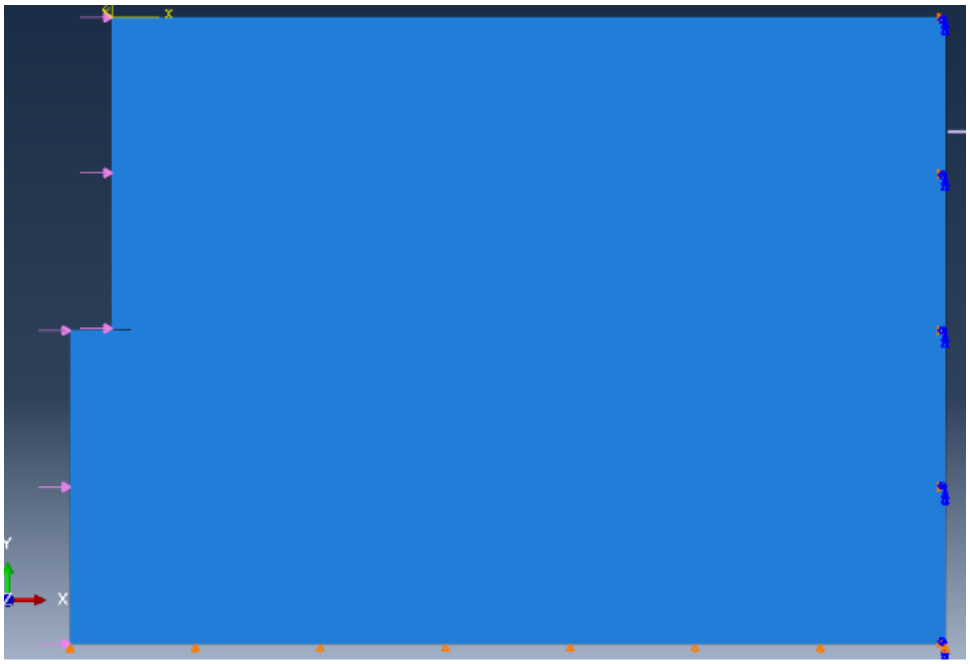

Figure 4.0.7: Well Model Showing Point of Pressure application and Boundary Conditions

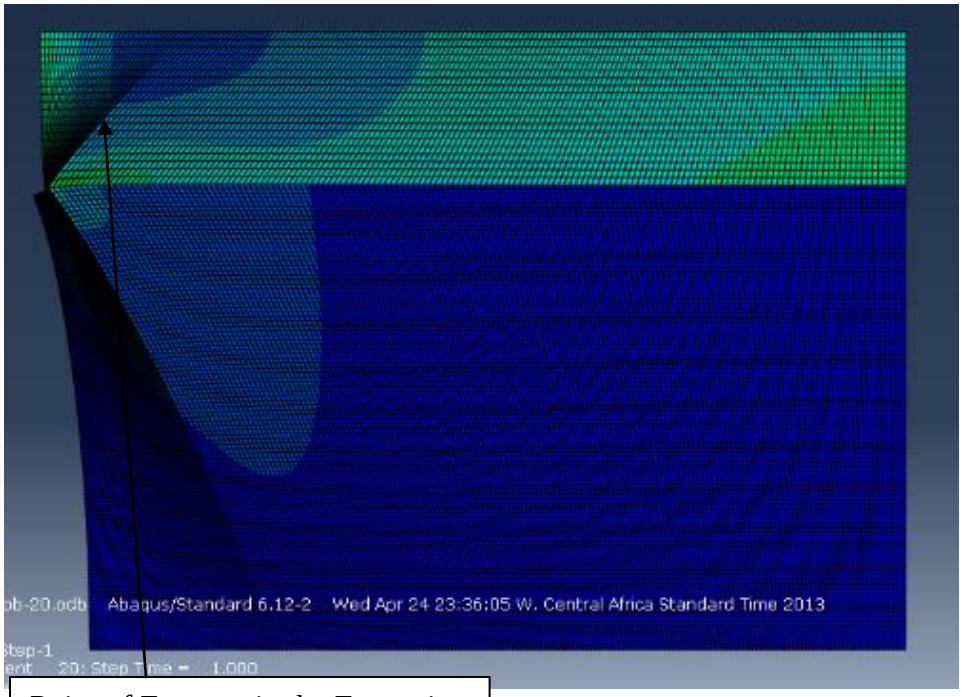

Figure 4.0.8: Model Showing Point of Fracture after Pressure application

4.6 J Integral for Interfacial Crack

Finite Element Method was used to obtain the J- integrals and the analytical solution presented in chapter 3, the effective stress intensity factor was obtained as presented in Table 4.0.3. The J-integral changes as a function of time, pressure and crack length. During simulation, J-integral values were generated at a time step of 0.05 seconds in steps of 20 to capture the field conditions under which pressure is applied.

Fracture at the interface occurs under mode-mixity with the occurrence of a critical value of J. The J- integrals computed are summarized in Table 4.0.3 below:

Table 4.0.3: J Integral for Interfacial Cracks

Pressure (Psi)	J Integral at Crack Length of 0.5 in	J Integral at Crack Length of 1.0 in	J Integral at Crack Length of 1.5 in	J Integral at Crack Length of 2.0 in	J Integral at Crack Length of 2.5 in
3000	2.2862	4.6875	5.0039	7.8670	10.7389
3500	3.1118	6.3800	6.8109	10.7078	14.6168
4000	4.0644	8.3333	8.8959	13.9857	19.0913
4500	5.1439	10.5468	11.2589	17.7006	24.1625
5000	6.3505	13.0207	13.8998	21.8526	29.8302
5500	7.6842	15.7551	16.8188	26.4417	36.0945
6000	9.1448	18.7498	20.0157	31.4678	42.9555
6500	10.7324	22.0050	23.4907	36.9310	50.4130
7000	12.4471	25.5206	27.2436	42.8312	58.4672
7500	14.2887	29.2966	31.2746	49.1684	67.1179

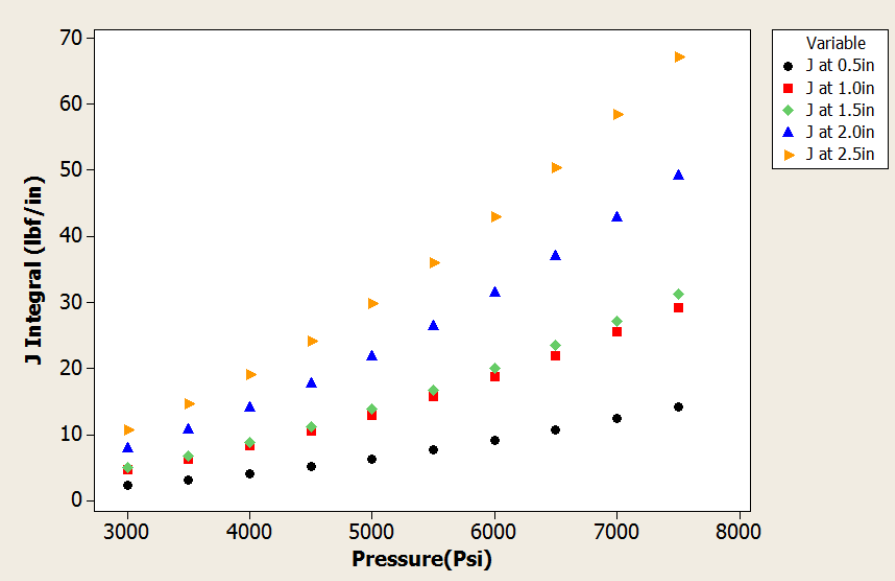

Figure 4.0.9 : Plot of J Integral at different crack lengths against Pressure

4.7 Variation of Upper Bound Drilling Pressure as Crack Length Changes

The upper bound pressure was determined by interpolation on the stress intensity factor-pressure plot. The pressure corresponding to J critical 9.09 lbf/in at a given crack length is the upper drilling pressure. Table 4.0.4 shows the change in pressure at different crack length.

Table 4.0.4: Upper Bound Mud Weight Drilling Pressure - Crack Length Data

Upper Mud Weigth Drilling Pressure (Psi)	Crack Length (in)
5832.21	0.5
4105.16	1.0
4005.18	1.5
3441.61	2.0
3184.37	2.5

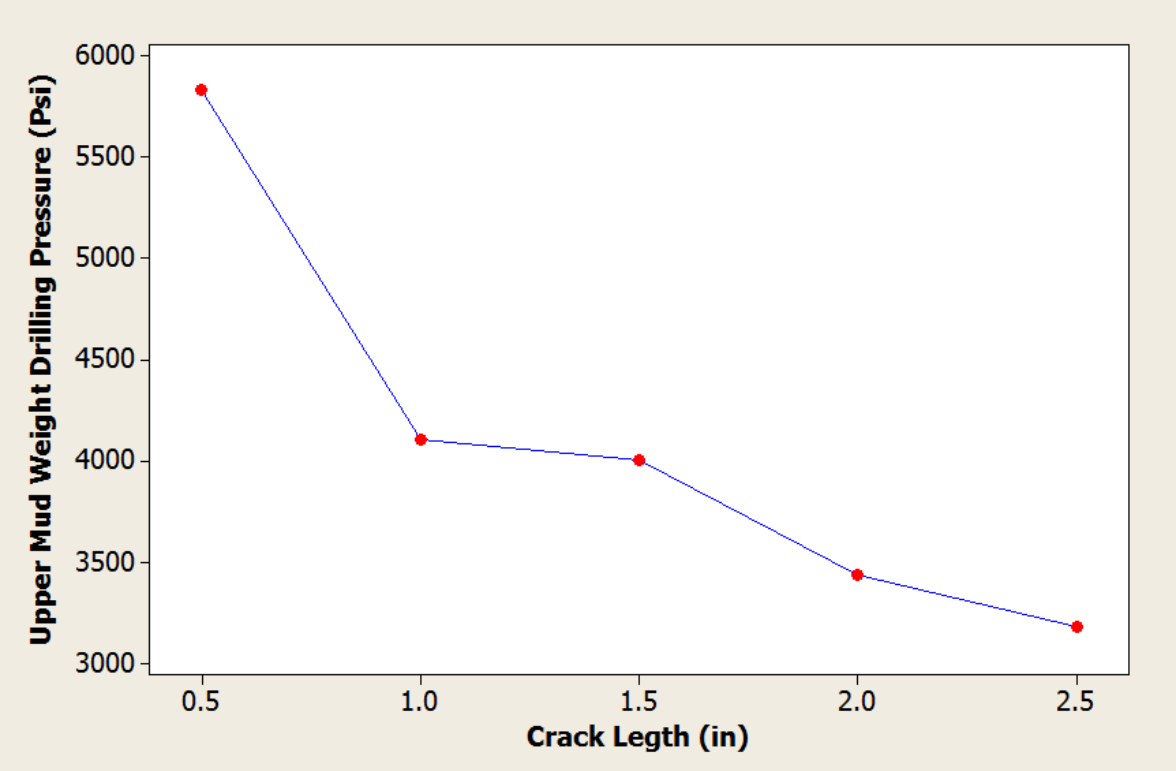

Figure 4.1.0: Plot of Drilling Pressure against Crack Length

4.8. Implications for Wellbore Stability Modeling

The result obtaining from the Finite Element Analysis as shown in results above implies a strong relationship between pressure and the stress intensity factor. This gives insight into how crack affect instability of well. This model can be incorporated into the design of mud weight pressure for safe drilling in the Niger Delta region.

REFERENCES

Fischer, M.P., 1994. Application of linear elastic fracture mechanics to some problems of fracture propagation in rock and ice. Ph.D. Thesis, The Pennsylvania State Univ., University Park, PA, 232 pp. (unpubl.).

Chapter 5

5.0 Conclusion and Future Work

5.1 Summary

This work involve the use of mechanical properties of shale from oil field data and literature to predict the upper bound drilling pressure by incorporating the properties into an $ABAQUS^{®}$ CAE 6.12 (teaching edition) software for numerical analysis.

5.2 Conclusion

The results from the Finite Element Analysis show that drilling pressure decreases as cracks in the wellbore propagate and also stress intensity factor increase as the drilling pressure increases.

5.3 Suggestion for Future Work

This work has been done with limited amount of oil field data. It is suggested that in the near future more data should be used so that analytical validation can be done using empirical theories.

It is also suggested that other physical phenomena such as chemical interactions and temperature should be factor into the model development. This will make the model more robust and relevant to the oil and gas industry.

APPENDIX: Oil Field Data

Shale/ Sand Name	**Bottom Shale/ Sand Depth**	**SHALE/ SAND THICKNESS**	**Top Shale/ Sand Depth**	**PRESSURE GRADIENT**	**UCS**	**YOUNG'S MODULUS**	**POISSON RATIO**	**COHESION**	**FRICTION ANGLE**	VERT	MAX	MIN
	fttvd			psi/ft		Mpa		Mpa	degrees	psi/ft	psi/ft	psi/ft
C4200	8240	250	8490	0.45	19.36	1936	0.25	6.1	25.38	0.908	0.838	0.788
C5000	8710	20	8730	0.45	29.85	2985	0.25	9.2	26.67	0.913	0.843	0.793
shale	9283	300	9583	0.45	15.35	1535	0.25	4.9	24.89	0.919	0.850	0.800
D1000 Shale	9753	200	9953	0.45	19.15	1915	0.25	6.1	25.36	0.923	0.856	0.806
D2000 Shale	10043	60	10103	0.45	19.15	1915	0.25	6.1	25.36	0.926	0.861	0.811
D6000 Shale	10347	380	10727	0.45	19.36	1936	0.25	6.1	25.38	0.929	0.865	0.815
D7000 Shale	10917	461	11378	0.45	26.13	2613	0.25	8.1	26.21	0.934	0.874	0.824
E1000 Shale	12584	80	12664	0.49	29.85	2985	0.25	9.2	26.67	0.947	0.903	0.853
E2000 Shale	13204	247	13451	0.49	41.07	4107	0.25	12.3	28.05	0.951	0.914	0.864
E3000 Shale	13614	100	13714	0.49	34.21	3421	0.25	10.4	27.21	0.954	0.922	0.872
E6000 Shale	14368	100	14468	0.49	54.28	5428	0.25	15.8	29.68	0.959	0.937	0.887
E7000 Shale	14498	72	14570	0.49	54.33	5433	0.25	15.8	29.68	0.960	0.939	0.889
E8000 Shale	14800	270	15070	0.49	41.08	4108	0.25	12.3	28.05	0.962	0.945	0.895
F1 Shale	15391	135	15526	0.765	41.69	4169	0.25	12.5	28.13	0.966	0.957	0.907
XF200 Shale	16152	16	16168	0.86	34.30	3430	0.25	10.5	27.22	0.970	0.973	0.923
XF3000 Shale	16296	578	16874	0.905	28.28	2828	0.25	8.8	26.48	0.971	0.976	0.926
XF4000 Shale	17002	75	17077	0.887	30.45	3045	0.25	9.4	26.75	0.975	0.990	0.940
TD	17077		17077	0.877	31.64	3164	0.25	9.7	26.89	0.976	0.992	0.942

* E1000 Shale parameters were used for interfacial crack modeling

Depth, ft	Water Depth, ft	Cohesion, psig	Friction Angle, deg	Poisson Ratio	Young's Modulus, Mpsi	Hole Diameter, in	Bit Diameter, in	OBG, psi/ft	Min Hor Stress, psi/ft
10000	6000	765	30	0.21	1.24E-06	8.5	9.875	0.96	0.72
12000	6000	765	30	0.22	1.24E-06	8.7	9.875	0.96	0.72
14000	6000	765	30	0.23	1.24E-06	8.9	9.875	0.96	0.72
16000	6000	765	30	0.24	1.24E-06	9.1	9.875	0.96	0.72
18000	6000	765	30	0.25	1.24E-06	9.3	9.875	0.96	0.72
20000	6000	765	30	0.26	1.24E-06	9.5	9.875	0.96	0.72
22000	6000	765	30	0.27	1.24E-06	9.7	9.875	0.96	0.72
24000	6000	765	30	0.28	1.24E-06	9.9	9.875	0.96	0.72
26000	6000	765	30	0.284	1.24E-06	10.1	9.875	0.96	0.72
28000	6000	765	30	0.286	1.24E-06	10.3	9.875	0.96	0.72
30000	6000	765	30	0.3	1.24E-06	10.5	9.875	0.96	0.72

Shale parameters in the table above were used for modeling crack within a layer